Bachelor's Thesis

## Bachelor's Degree in Industrial Engineering

# Control and Simulation of Photovoltaic Power Plants in OpenModelica

**Author:** Lluc Figueras Llerins

**Director:** Eduardo Prieto Araujo

**Date:** June 2020


Escola Tècnica Superior

d'Enginyeria Industrial de Barcelona

# Abstract

As solar generation increases globally, there exists a need for innovation and increased operational flexibility. In Photovoltaic Power Plants (PVPPs) and Large Scale Photovoltaic Power Plants (LS-PVPPs) the challenges increase due to the necessity to integrate them into the electrical system. To ensure the stability and reliability in the electricity supply, power systems require complex dynamic analysis. Therefore, to carry out these analysis, modelling and simulation tools are needed. This thesis focuses on the control and operation of PVPPs in OpenModelica, a free and open-source modelling and simulation environment based on Modelica language. In the later part, OpenModelica potential in large-scale power system-oriented models is investigated. These issues are addressed by a literature review concerning photovoltaic power systems and OpenModelica functionality, a theoretical analysis of a photovoltaic inverter and a LS-PVPP, and detailed simulations. The models are tested under variations in the active and reactive power requirements. The results show an optimal dynamic response and the capacity to perform independent active and reactive power controls. As an outcome, OpenModelica is a promising tool for power system modelling and simulation even though existing barriers and difficulties must be overcome.

# Contents

# List of Figures

# List of Tables

# Nomenclature

## List of symbols

| | |
|---|---|
| $E_{DC}$ | VSC DC-side voltage |
| $E_m$ | Admitted peak voltage |
| $f$ | AC grid frequency |
| $f_{sw}$ | Switching frequency |
| $\theta_{PLL}$ | Phase Locked Loop angle |
| $i_{abc}$ | Currents in abc frame |
| $I_{DC}$ | VSC DC-side current |
| $i_q, i_d$ | VSC q-axis current, VSC d-axis current |
| $i_q^*, i_d^*$ | VSC inner-current controller q-axis reference, VSC inner-current controller d-axis reference |
| $k_i^{icc}$ | Inner current controller integral gain |
| $k_i^{oc}$ | Outer current controller integral gain |
| $k_i^{PLL}$ | Phase Locked Loop integral gain |
| $k_i^{ppc}$ | Power plant controller integral gain |
| $k_p^{icc}$ | Inner current controller proportional gain |
| $k_p^{oc}$ | Outer controller proportional gain |
| $k_p^{PLL}$ | Phase Locked Loop proportional gain |
| $k_p^{ppc}$ | Power plant controller proportional gain |
| $\xi$ | Damping ratio |
| $l_l$ | Converter coupling inductance |
| $N_{PV_{inv}}$ | Number of PV inverters in the PVPP |
| $P^*$ | Active power reference |

| | |
|---|---|
| $P_{AC}$ | VSC AC-side calculated active power |
| $P_{DC}$ | VSC DC-side calculated active power |
| $P_{min}, P_{max}$ | Allowable active power in the PVPP |
| $P_{PVPP}$ | Measured active power at the PCC |
| $P_{ref}$ | Active power reference to give to each PV inverter |
| $P_{TSO}$ | Active power required by the TSO |
| $Q^*$ | Reactive power reference |
| $Q_{min}, Q_{max}$ | Allowable reactive power in the PVPP |
| $Q_{PVPP}$ | Measured reactive power at the PCC |
| $Q_{ref}$ | Reactive power reference to give to each PV inverter |
| $Q_{TSO}$ | Reactive power required by the TSO |
| $r$ | Line resistance |
| $r_l$ | Converter coupling resistance |
| $S_n$ | Nominal power |
| $T(\theta)$ | Park transformation |
| $T^{-1}(\theta)$ | Inverse Park transformation |
| $\tau_{icc}$ | Inner current controller time constant |
| $\tau_{oc}$ | Outer controller time constant |
| $\tau_{PLL}$ | Phase Locked Loop time constant |
| $\tau_{ppc}$ | Power plant controller time constant |
| $v_{abc}$ | Voltage in abc frame |
| $V_{conv}$ | Converter voltage |
| $v_q, v_d$ | VSC q-axis voltage, VSC d-axis voltage |
| $v_q^*, v_d^*$ | VSC q-axis reference voltage, VSC d-axis reference voltage |
| $v_l^0$ | VSC AC-side neutral point |
| $v_l^{abc}$ | VSC AC-side voltage abc frame |
| $V_p$ | Primary voltage |
| $V_{RMS}$ | Line to line voltage |
| $V_s$ | Secondary voltage |

| | |
|---|---|
| $V_t$ | Tertiary voltage |
| $v_z^0$ | Grid neutral point |
| $v_z^{abc}$ | Grid voltage abc frame |
| x | Line reactance |
| $\omega_e$ | Electrical grid angular velocity |

## List of acronyms

| | |
|---|---|
| AC | Alternating Current |
| BDEW | German Association of Energy and Water Industry |
| BLT | Block Lower Triangular |
| DAE | Differential Algebraic Equation |
| DC | Direct Current |
| EU | European Union |
| FMI | Functional Mock-up Interface |
| HPCOM | High Performance Computing OpenModelica |
| HV | High Voltage |
| IGBT | Insulated Gate Bipolar Transistor |
| IMC | Internal Model Control |
| LS-PVPP | Large Scale Photovoltaic Power Plant |
| LV | Low Voltage |
| MV | Medium Voltage |
| ODE | Ordinary Differential Equation |
| OM | OpenModelica |
| OMC | OpenModelica Compiler |
| PCC | Point of Common Coupling |
| PI | Proportional-integral controller |
| PLL | Phase Locked Loop |

| | |
|---|---|
| PPC | Power Plant Control |
| PV | Photovoltaic |
| PVPP | Photovoltaic Power Plant |
| PWM | Pulse Width Modulation |
| SVPWM | Space Vector Pulse Width Modulation |
| TLM | Transmission Line Modelling |
| TSO | Transmission System Operator |
| VSC | Voltage Source Converter |

# Preface

The burning of fossil fuels to provide energy supply is still the largest source of the world's greenhouse gas emissions, representing 68% of the total amount according to the European Commission [1].

Nowadays, renewable energy is increasing its importance in the energy mix of most countries. In particular, photovoltaic technology is becoming more widely used globally and represents a bigger part of the European Union energy mix. It is a powerful technology to develop a decarbonized power sector and sustainable energy supply. Between 2010 and 2018 the benchmark average net cost of electricity from photovoltaic systems decreased by over 75% [1]. In 2018, the EU output of photovoltaic electricity reached 127 TWh, amounting to nearly 4% of its gross electricity production [2]. Additionally, in 2019 the solar market has increased over 100% in the EU, more than any other power generation technology [3].

However, as solar generation increases globally, there exists a need for innovation and increased operational flexibility. In Photovoltaic Power Plants (PVPPs) and Large Scale Photovoltaic Power Plants (LS-PVPPs), the challenges increase as a result of the necessity to integrate them into the electrical system. Due to the variability of renewable resources, without adequate control, PVPPs can not be adequately integrated into the electrical grid as conventional power plants do.

To ensure the stability and reliability in the electricity supply, power systems require complex dynamic analysis. Therefore, to carry out these analysis, modelling and simulation tools are needed.

# Chapter 1

# Introduction

This chapter addresses a literature review about photovoltaic (PV) power systems with the focus in grid connected systems. PVPPs internal configuration, collection grid topologies and electrical components as inverters and transformers are presented. The design and simulation of the models of study are developed in OpenModelica. Therefore, new approaches and new trends to handle large-scale Modelica power systems-oriented models are described together with available modelling concepts and parallel simulation capabilities. Finally, the thesis objectives and research questions are detailed.

## 1.1 Photovoltaic Power Systems

The PV power systems are commonly classified according to their operational requirements, configuration and connection to other power sources or electrical loads [4].

### 1.1.1 Stand-alone PV systems

Stand-alone PV systems are intended to be used in off-grid applications. Are an economical and efficient electricity supply for rural area customers or locations where grid expansion is complicated and expensive [5].

### 1.1.2 Hybrid PV systems

Hybrid PV systems consist of a combination of a PV module and complementary engine-driven storage and/or battery storage. They offer high flexibility and reliability compared to stand-alone PV systems due to the two or more different energy sources. Therefore, hybrid systems often require more complex controls than stand-alone PV systems.

### 1.1.3 Grid connected PV systems

Grid connected PV systems represent 99% of the overall power installed, compared to stand-alone systems [6]. Grid connected PV power generation systems are commonly divided

according to their power rating: small scale, medium scale and large scale [7]. Generally, small scale systems generate less than 100 kW and are used in residential applications. Then, medium scale systems generate between 100 kW and 1MW and are located in small PV farms. Finally, large scale systems comprise power levels from 1 MW to hundreds of MW [6].

The integration of LS-PVPPs into the utility grid can have a significant impact on its stability and operation. Hence, many countries have established new requirements for grid integration of LS-PVPPs to permit a smooth interaction between the electrical system and these power plants [8]. Grid codes define the mandatory requirements for power system operation in order to maintain the stability and reliability of the transmission system. The first grid code exclusively for PVPPs and LS-PVPPs interconnected with the transmission grid was set in 2008 in Germany by the German Association of Energy and Water Industry (BDEW) [9]. Grid codes have been adapted considering the increase in PV generation. Hence, updated grid codes demand that LS-PVPPs provide ancillary services such as fault ride-through, active and reactive power management and voltage and frequency support to ensure a more reliable and secure grid [10]. Therefore, the principal technical challenges for the interconnection of these plants to the electrical system are [11]: (i) active power control, (ii) frequency support, (iii) reactive power control and (iv) voltage support.

## 1.2 Photovoltaic Power Plant configuration

Photovoltaic output power depends on the connection of the internal components and the collection grid configuration. According to the system location, cost, reliability and power rating a certain internal connection topology and AC collection grid topology will be selected.

### 1.2.1 Internal connection topology

The connection between the PV panels with PV inverters and transformers comprises three basic topologies: central, string, and multi-string [12,13]. The configuration is chosen in each particular case regarding the power output, location, cost, efficiency, and reliability. In PVPPs and LS-PVPPs, the most widely implemented technology is the central PV inverter configuration connected to the internal power plant grid through a three-winding transformer (Fig. 1.1) [6]. In this case, the power rating ranges from 0.1 to 1.5 MW and the output AC voltage is comprised between 270 and 400 V [14].

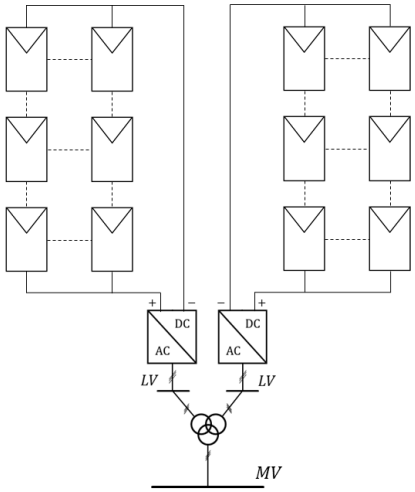


Figure 1.1: Central PV inverter topology

### 1.2.2 Collection grid topology

Regarding collection grid topologies for PVPPs and LS-PVPPs, they have been very little documented. However, collection grid topologies can be divided into three main technologies: radial, string, and star [14]. In the star collection topology, each inverter is connected directly to the main feeder or collector (see Fig. 1.2). This topology reduces cable lengths aiming to have similar losses between them. This configuration offers high system reliability but at a high cost.

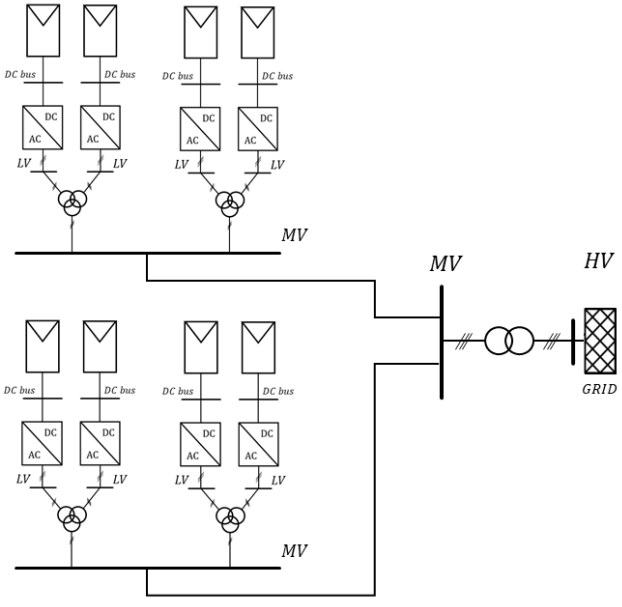


Figure 1.2: Star collection grid configuration

## 1.3 Electrical components

The electrical components of PVPPs are in charge of converting solar energy to electricity, connecting the plant to the grid and assuring a suitable performance. Two of the main components involved in this duty are photovoltaic inverters and transformers.

### 1.3.1 PV inverters

The PV inverters are power electronic devices that convert direct current to alternating current. In the case of PVPPs, the PV inverters generate alternating grid-compliant current from the PV modules. The typically established inverter topologies are the neutral point clamped (NPC) and the cascaded H-bridge (CHB) [15].

Currently, the most used technology in commercial PVPPs and LS-PVPPs is the one stage DC-AC [16]. The principal duties of a PV inverter are to provide a low-loss conversion, a power optimization, temperature management, and reliable monitoring both of the power plant yield and the power grid [17]. In the recent years, interest in PV inverters that can support ancillary services has grown, which is a crucial aspect to overcome the challenges caused by the growth of LS-PVPP connected to the electrical system [10].

### 1.3.2 Transformers

In most PVPPs and LS-PVPPs, there are two types of transformers. The first one increases the voltage from the inverter output low voltage (LV) to medium voltage (MV) ranging from 13.8 kV to 46 kV [18]. Commonly, if the PV inverter has a power rating above 0.5 MW a three-winding transformer is used [20]. This transformer consists of one medium voltage winding in the primary and two low voltage windings in the secondary and tertiary. The existing vector groups are [19]: $Dy_ny_n$, $Dd_nd_n$, $Yd_nd_n$, $YNy_ny_n$ and $YNd_nd_n$. The second one steps up the voltage from medium voltage to high voltage (HV), connects the PVPP to the grid, and provides galvanic isolation. The existing vector group is Yy.

## 1.4 OpenModelica

OpenModelica is an open-source modelling and simulation environment intended for industrial and academic usage based on Modelica language. Its long-term development is supported by a non-profit organization – the Open Source Modelica Consortium [21]. Modelica language is a non-proprietary, object-oriented, equation-based language to conveniently

model complex cyber-physical systems [22,23]. Consider that OpenModelica is in continuous development.

Current power systems modelling and simulation tools are very powerful but with their own format and structure. Therefore, instead of imposing a modelling tool, a common language can be proposed. Equation-based languages such as Modelica can be used to disconnect the dependency between the power system tool and the power system model, and to provide an open standard implementation. Hence, Modelica-based models can be exchanged and validated between different Modelica tools.

### 1.4.1 Solving large-scale Modelica power system-oriented models

Modelica capability to build larger and more complex models is increasing. Therefore, is crucial to focus on the quality of the solvers to handle large-scale models and stiff electrical systems. In [24] the open-source power systems libraries available are reviewed (2017).

OpenModelica solvers, when confronted with large-scale models with a significant number of algebraic systems of equations (more than 1000 unknowns) or a high number of states (more than 1000), can confront serious efficiency issues. The authors of [25] present the state of the art and future perspectives in solving large-scale Modelica models together with some promising research trends to address the challenges of efficient simulation of these models.

A feasibility study of the modelling and simulation of large-scale electrical power systems using Modelica is conducted in [26]. The authors of [27] carry out an analysis of simulation speed and improvements of Modelica models for building energy systems. An approach to speed up Modelica models simulation is presented.

More recently, in [28] newly implemented techniques and strategies to efficiently compile and simulate large-scale Modelica models are exposed together with its experimental results. The system size of Modelica-based models is continuously increasing and the conventional way of generating simulation code including e.g. matching and index reduction, sorting, and tearing, must be adjusted to this trend.

By default, OpenModelica transforms a Modelica model into an Ordinary Differential Equation (ODE) representation to perform a simulation by using numerical integration methods [29]. However, in order to speed up the compilation and simulation, Differential Algebraic Equation (DAE) solvers can be employed as an alternative to ODE solvers. In power systems simulations, tests have shown that DAE solvers can have better performance and be several orders of magnitude faster than traditional ODE solvers when simulating models with large algebraic loops, such as power grid models [30]. The whole equation system of a model is passed to the DAE integrator which reduces the workload in the post-optimization phase of the OpenModelica Compiler (OMC) back-end [29]. In [31] the authors claim a strategy for DAE mode simulations of large-scale electrical models is presented. Nevertheless, the outcome of using DAE or ODE mode highly depends on each specific case [28]. The authors of [32] discuss

the use of the DAE mode in industrial power systems simulations in OpenModelica and its future perspectives.

Last year, a possible roadmap to towards a high-performance Modelica compiler to achieve high efficiency and optimization in simulation execution was presented in [33]. Finally, the current possibilities for solving Modelica models are described in [29].

### 1.4.2 FMI and TLM-Based Simulation and Co-simulation

The fundamental concept of Transmission Line Modelling (TLM) is based on modelling a system in a way that the components can be somewhat numerically independent from each other. This permits to each component or subsystem to solve its own equations independently of the rest of the system. The current centralized solvers algorithms restrict often the possibilities to speed up simulations. Through distributed solver algorithms using the Transmission Line Modelling (TLM) method, the computation time could be decreased by an efficient distributed simulation [34]. However, TLM may be unsuitable for very stiff systems, such large electrical systems with a high number of resistors, inductances or capacitors connected to each other [35].

Currently, OpenModelica is working to provide a generalized simulation framework based on the Functional Mock-up Interface (FMI) co-simulation and TLM-based interfaces [36]. The OMSimulator is a FMI-based co-simulation tool that supports ordinary and TLM connections. Large-scale simulations using models from multiple sources using the FMI standard are supported [37]. For example, sharing dynamic system models between different simulation environments such as Matlab-Simulink® and OpenModelica.

### 1.4.3 Parallelization of equation-based Modelica models

The size and complexity of modelled systems are continuously increasing. These models require a high-performance execution to obtain acceptable simulations execution times. Constant advances in multi-core CPU's offer high computational power. Hence, to take advantage of the available computational power, modern modelling environments need to provide different parallelization and optimization options. The main idea behind parallelization is to divide the computational work between the processors of a multi-core system to speed up simulations. However, parallelization of equation-based object-oriented languages is not an easy task.

Regarding the Modelica community, most of the attempts in this direction come from Linköping University PELAB. There have been a few parallelization capabilities in OpenModelica, some of them still work. Others are obsolete and some are being improved.

Manual parallelization approaches can be error-prone, tedious and may require previous knowledge about parallel programming language even though the users working on different areas may not have knowledge about it. Therefore, an automatic parallelization approach would be suitable. The author of [38] presents solutions to the research problem regarding automatic parallelization methods in equation-based object-oriented languages with the focus in the Modelica context.

Following the same strategy that was put forward in [38], the author of [39] presents an algorithm to distribute over parallel CPU cores the solution of the DAEs stemming from object-oriented models that can be effective in the case of generalized physical networks. It is suggested to build a task graph parallelization based on the Block Lower Triangular (BLT) representation of a model. More recently, in [40] the ideas exposed in [39] are implemented into the OMC and evaluated, followed by the comparison of the different scheduling algorithms efficiency.

Currently, regarding OpenModelica, the first available alternative is the HPCOM implementation [41], based on Task-Graph-Based Parallelization. However, it is still under construction and may not be fully operational. In [42] selected models have been tested using this method and has shown that is able to speed up simulations for some models, even though for electrical systems further research is required.

The authors of [43] present a technology to automatically parallelize Modelica model equations together with an electrical example that is discussed in detail. In [34] another automatic parallelization approach using TLM is presented. However, this approach is not generally applicable, even when applicable or suitable, concerning parallelization, it requires specific way of modelling according to [44]. Moreover, this approach highly depends on the modeller, that must introduce the appropriate TLM components in the model to obtain performance benefit [39].

Finally, the ParModelica parallelization implementation [44] is currently being updated and integrated into the current OMC. The master branch it is supposed to be merged soon.

## 1.5 Objectives and Research Questions

The aim of this thesis is to develop a LS-PVPP model and its control system in OpenModelica. Thus, explore OpenModelica as an open-source alternative to commercial software in power and control systems. Moreover, investigate its robustness and scalability in modelling large-scale electrical systems. The main objectives can be summarized as:

- Design a PV inverter model based on the Voltage Source Converter
- Design a 128 MW Large Scale Photovoltaic Power Plant model based on real industry case
- Simulate both designed models and analyse their dynamic behaviour under variations in the active and reactive power requirements
- Explore OpenModelica potential in large power system-oriented models simulation and investigate parallelization capabilities

The design and simulation of the different studies are developed exclusively in OpenModelica.

Therefore, the work conducted on this thesis is intended to answer the following research questions:

1. How the dynamic response of a Voltage Source Converter a is affected by variations of the active and reactive power reference values?

2. How the dynamic response of a LS-PVPP is affected by the active and reactive power set-points required by the Transmission System Operator?

3. Can OpenModelica become a reliable and capable simulation tool to study the proposed power systems and large-scale electrical models?

# Chapter 2

# System modelling

This chapter presents the theoretical aspects to build the different systems and models in OpenModelica. The chapter focuses on three main elements: the PV inverter and its local control system; the PV generator configuration that consists of two inverters connected to the internal PVPP grid through a three-winding transformer; and a model and control system of a LS-PVPP.

In this study, both the PV inverter and the LS-PVPP are operated in the PQ mode in such a way that they follow defined active and reactive power set-points.

## 2.1 PV inverter model

The PV inverter under analysis is a Voltage Source Converter (VSC). The VSC is able to control independently active and reactive power and to inject reduced harmonic currents to the grid permitting the use of light filters [45]. It is based on Insulated-Gate Bipolar Transistors (IGBTs) in order to provide fast switching frequency to modulate the desired output voltage. As shown in Fig. 2.1, it consists of three parallel branches or legs, one per phase, and two IGBT switches in each branch. The middle point of each branch is connected to the grid through an inductive filter.

Therefore, considering computation time, because of the need to set a very low simulation step-size due to the relatively high switching frequency, that will lead to low simulation speed, an average value model of the VSC will be used.

The average model is derived decoupling the DC and AC sides of the converter as represented in Fig. 2.1. The DC side is modelled as a current source and a capacitor while the AC side is replaced by a three-phase voltage source controlled by the converter control system. Assuming the VSC lossless model, the power balance can be computed as

$$I_{DC} = \frac{P_{DC}}{E_{DC}} = \frac{P_{AC}}{E_{DC}} \tag{2.1}$$

where $E_{DC}$ is the DC bus voltage and $P_{AC}$ is the active power exchanged between the grid and the converter.

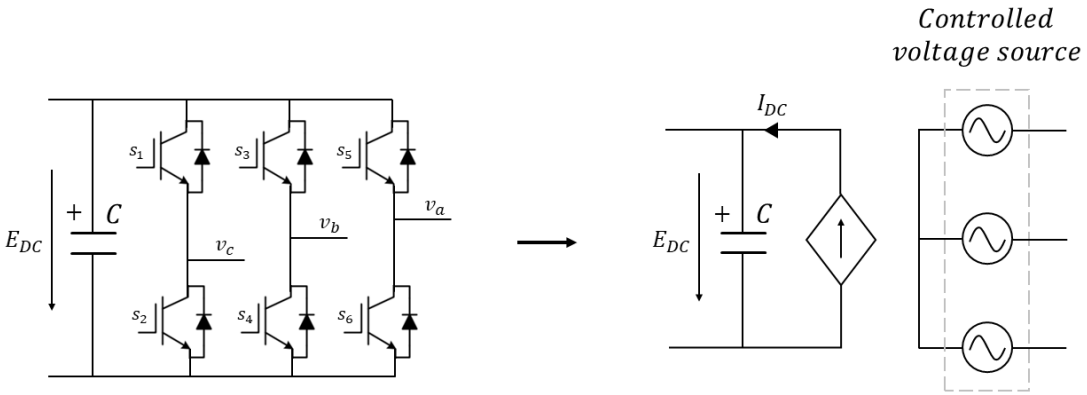


Figure 2.1: Voltage Source Converter average model

## 2.2 Dynamic control

The control scheme of the VSC is based on a cascade control system. The design of the controllers is carried out by the Internal Model Control (IMC) method [46, 47]. Basically, it consists on cancelling the internal dynamics of the plants and impose the desired ones. This control enables the converter to inject the required active and reactive power to the grid.

The traditional vector control is the most widely used control method of VSCs, where the three-phase currents and voltages are transformed into the rotating direct-quadrature synchronous reference frame. The VSC local control scheme is shown in Fig 2.2. This control consists of a Phase Locked Loop (PLL), an inner current control, a voltage modulation block, and an outer control. The inner loop is designed to achieve short settling times while the outer loop purpose is to attain optimal regulation and stability. Both the current loop and the power loop are set to follow first order dynamics.

The DC side of the converter has been modelled and a DC voltage regulator has been tested. However, in the following sections it is considered as a fixed $E_{DC}$ voltage source.

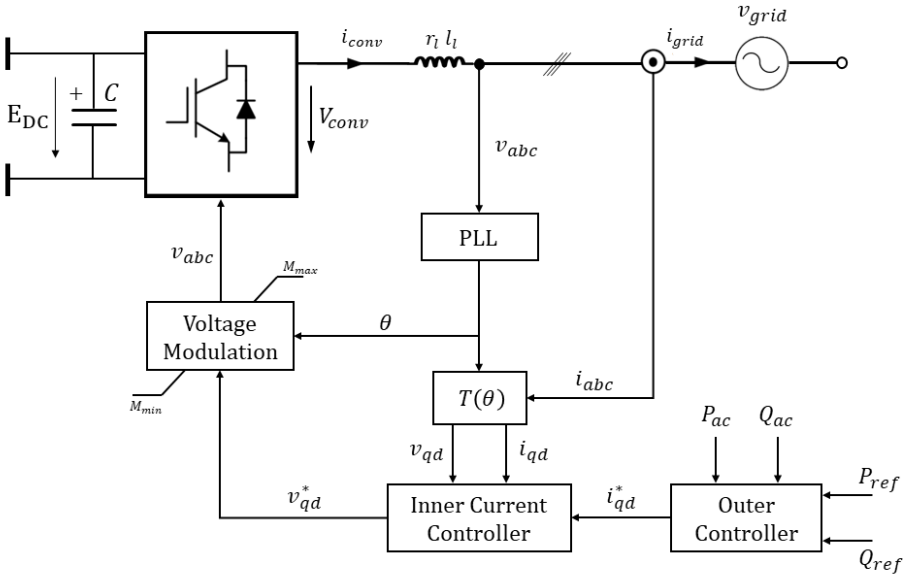


Figure 2.2: Inverter local control scheme

### 2.2.1 Instantaneous power theory in the synchronous reference frame

Considering the instantaneous power theory in the synchronous reference frame, which consists in transforming the voltages in the $abc$ frame to the $qd0$ domain using the Park transformation, the apparent power of a three-phase system is [45]:

$$\underline{S} = P + jQ = 3 \cdot \underline{V}^{qd} \cdot \underline{I}^{qd*} \tag{2.2}$$

Decomposing the real and the complex parts, the active and reactive power can be expressed as functions of the voltages and currents in the $qd0$ frame:

$$P = \frac{3}{2} \cdot \left(v_q \cdot i_q + v_d \cdot i_d\right) \tag{2.3}$$

$$Q = \frac{3}{2} \cdot \left(v_q \cdot i_d - v_d \cdot i_q\right) \tag{2.4}$$

If the PLL is suitably synchronized with the system then $v_z^d$ is equal to zero. Consequently, the current references can be expressed as

$$i_q^* = \frac{2}{3} \cdot \frac{P^*}{v_z^q} \tag{2.5}$$

$$i_d^* = \frac{2}{3} \cdot \frac{Q^*}{v_z^q} \tag{2.6}$$

where $P^*$ and $Q^*$ are the active and reactive power references.

### 2.2.2 Phase Locked Loop

The Phase Locked Loop technique is a method used to synchronize the phase angle between the converter reference $qd0$ frame and the grid $qd0$ frame [48]. It uses a PI controller to compensate the error between the reference $v_d^*$ and the calculated $v_d$ (Fig. 2.3)

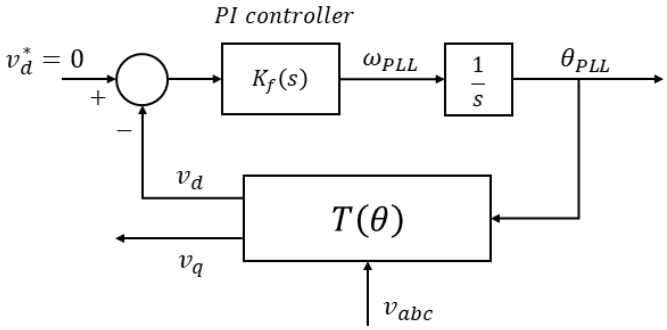


Figure 2.3: Phase Locked Loop

In order to design the PLL controller, the system is linearized assuming the small-angle approximation. The controller can be defined as [49]

$$K_f(s) = k_p^{PLL}\left(\frac{\frac{1}{\tau_{PLL}} + s}{s}\right) \tag{2.7}$$

where $\tau_{PLL}$ is the PLL time constant. The PI parameters can be determined by

$$\xi = \frac{\sqrt{\tau_{PLL} k_p^{PLL} E_m}}{2} \tag{2.8}$$

$$\omega_e = \sqrt{\frac{k_p^{PLL} E_m}{\tau_{PLL}}} \tag{2.9}$$

where $E_m$ is the admitted peak voltage value, ξ is the desired damping ratio and $\omega_e$ is the angular velocity of the electrical grid.

### 2.2.3 Inner Current Control

The inner current control determines the reference voltages that must be applied to the converter. The converter voltage equations can be obtained using the equivalent scheme illustrated in Fig. 2.4.

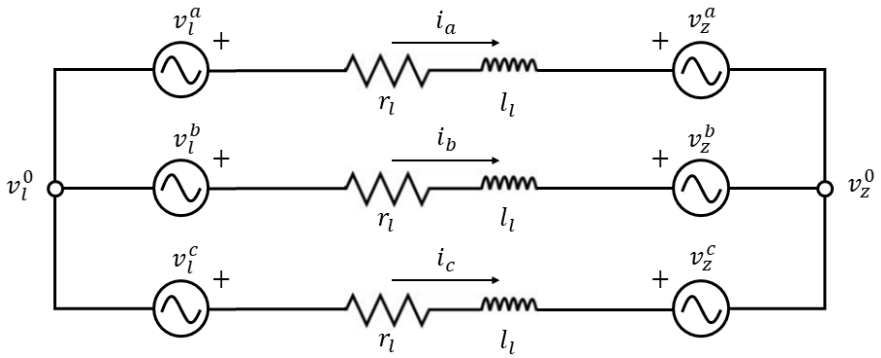


Figure 2.4: Average model of the converter AC side

The system equations without the neutral point can be expressed in the matrix form as

$$v_l^{abc} - v_z^{abc} = \begin{bmatrix} r_l & 0 & 0 \\ 0 & r_l & 0 \\ 0 & 0 & r_l \end{bmatrix} i_{abc} + \begin{bmatrix} l_l & 0 & 0 \\ 0 & l_l & 0 \\ 0 & 0 & l_l \end{bmatrix} \frac{d}{dt} i_{abc} \tag{2.10}$$

and in the synchronous reference frame as

$$\begin{bmatrix} v_l^q - v_z^q \\ v_l^d - v_z^d \end{bmatrix} = \begin{bmatrix} r_l & l_l \cdot \omega_e \\ -l_l \cdot \omega_e & r_l \end{bmatrix} \begin{bmatrix} i_q \\ i_d \end{bmatrix} + \begin{bmatrix} l_l & 0 \\ 0 & l_l \end{bmatrix} \frac{d}{dt} \begin{bmatrix} i_q \\ i_d \end{bmatrix} \tag{2.11}$$

Where $v_l^q$ and $v_l^d$ are the converter voltages, $v_z^q$ and $v_z^d$ are the grid voltages, $i_q$ and $i_d$ are the currents in the $qd0$ reference and the $\omega_e$ is the angular velocity of the grid. Notice that there exists a cross-coupling between $i_q$ and $i_d$. To overcome the cross-coupling a feedback loop control is used. Since the control is designed to decouple the currents that in the synchronous reference frame are originally coupled, the following decoupled structure is proposed to compensate the dynamic coupling between the two control loops [46, 47]:

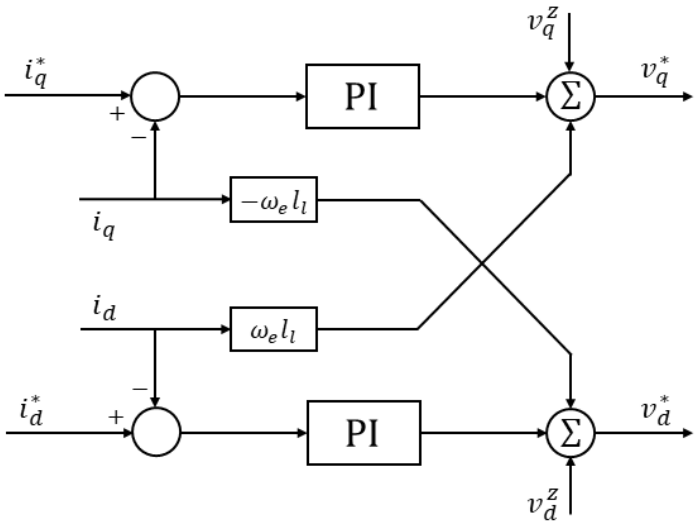


Figure 2.5: Inner Current Controller

Finally, the converter is able to produce the desired voltages by setting the decoupled expressions

$$\begin{bmatrix} v_q^* \\ v_d^* \end{bmatrix} = \begin{bmatrix} \hat{v}_l^q + v_z^q + l_l \cdot \omega \cdot i_d \\ \hat{v}_l^d + v_z^d - l_l \cdot \omega \cdot i_q \end{bmatrix} \tag{2.12}$$

where $\hat{v}_l^q$ and $\hat{v}_l^d$ are the outputs of the PI controller. The controller is given by

$$F(s) = k_p^{icc} + \frac{k_i^{icc}}{s} = \frac{l_l}{\tau_{icc}} + \frac{r_l}{\tau_{icc} \cdot s} \tag{2.13}$$

Then comparing both expressions the PI parameters can be stated as

$$k_p^{icc} = \frac{l_l}{\tau_{icc}} \tag{2.14}$$

$$k_i^{icc} = \frac{r_l}{\tau_{icc}} \tag{2.15}$$

where $\tau_{icc}$ is the closed loop current controller time constant and $l_l$ and $r_l$ are the converter coupling inductance and coupling resistance.

### 2.2.4 Voltage modulation

The voltage modulation block transforms the reference voltages $v_q^*$ and $v_d^*$ provided by the inner current control with the corresponding modulation technique to supply the required three phase voltage $v_{abc}$ to the converter. The VSC is able to apply the reference voltages by modulating them using Pulse Width Modulation (PWM) techniques. However, as stated before the thesis will be conducted using an average value model. Therefore, the implemented averaged voltage modulation block is shown in Fig. 2.6 where $0 \leq M \leq 1$ is the modulation index.

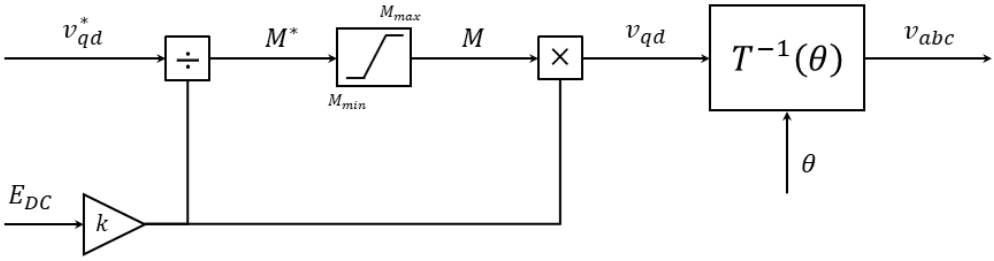


Figure 2.6: Voltage Modulation block

However, in appendix B, Space Vector Pulse Width Modulation (SVPWM) is presented together with its Modelica implementation.

### 2.2.5 Outer control

The outer controller is responsible for the active and reactive power control which determines the current references, $i_q^*$ and $i_d^*$, for the inner current controller. A closed-loop control is used to regulate the power injected into the grid. The active and reactive power are measured after the inverter filters and their values are compared with their references. Then, PI-based controllers compute the $i_q^*$ and $i_d^*$ reference currents as shown in Fig. 2.7.

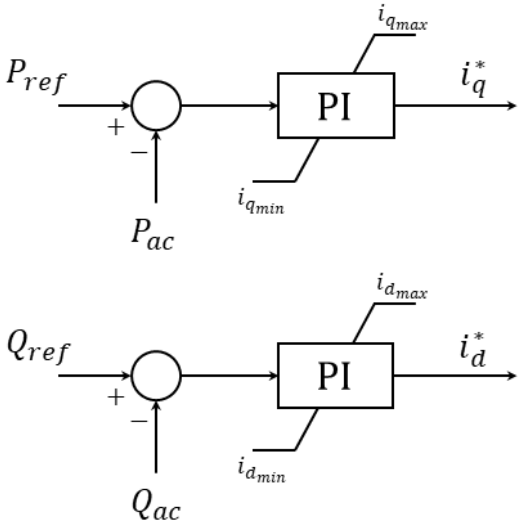


Figure 2.7: Active and reactive power controller

Concerning the controller design, due to the general cascade control applied, the outer controller time constant must be slower than the lower control system. The $v_z^q$ grid voltage variations are considered negligible and the $v_z^d$ is not taken into account due to the PLL setting.

The controller is given by

$$F(s) = k_p^{oc} + \frac{k_i^{oc}}{s} = \frac{\tau_{icc}}{\tau_{oc} \cdot \frac{3}{2} \cdot v_z^q} + \frac{1}{\tau_{oc} \cdot \frac{3}{2} \cdot v_z^q \cdot s} \tag{2.16}$$

Then comparing both expressions the PI parameters can be stated as

$$k_p^{oc} = \frac{\tau_{icc}}{\tau_{oc} \cdot \frac{3}{2} \cdot v_z^q} \tag{2.17}$$

$$k_i^{oc} = \frac{1}{\tau_{oc} \cdot \frac{3}{2} \cdot v_z^q} \tag{2.18}$$

where $\tau_{oc}$ is the outer controller time constant.

## 2.3 PV generator model

The proposed PV generator consists of two PV inverters connected to the internal PVPP grid through a three-winding transformer as mentioned in Section 1.2. The three-winding transformer must be designed for asymmetrical load flow in the low voltage systems to ensure permanent operation and for feed-in with one single inverter [19].

A Dy1y1 vector group transformer is implemented, according to SMA [19]. As can be seen in Fig. 2.8 both low voltage windings are connected in star configuration (Y) while the medium voltage winding is connected in delta configuration (D). The D structure has its voltages lagging 30 degrees in comparison to the voltages in the Y windings.

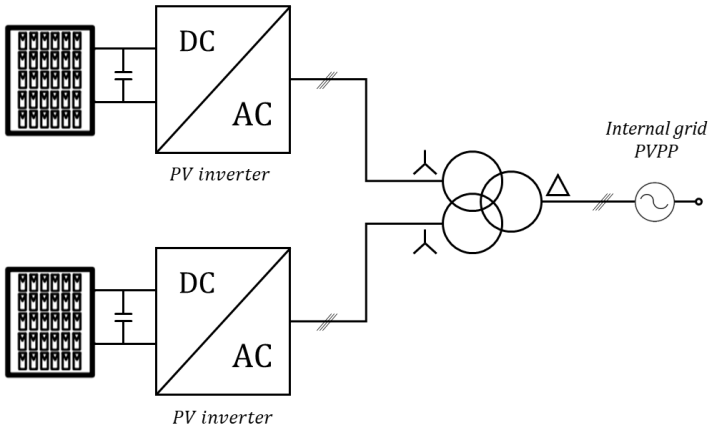


Figure 2.8: PV generator configuration

## 2.4 Large Scale Photovoltaic Power Plant

Even though there is no clear classification on PV power plant size regarding the installed capacity, the considered one in this study could be classified as LS-PVPP, ranging from several megawatts to gigawatts [50,51]. The PV plant model taken as a reference is the Templin Photovoltaic Power Plant in Brandenburg, Germany, which aims to provide renewable energy to the greater Berlin area.

### 2.4.1 Power Plant configuration

The Templin Photovoltaic Power Plant covers a total area of 214 ha [52] and consists of 114 SMA Sunny Central 900CP XT PV inverters with a total peak power of 128 MWp [53]. The PV inverters are grouped in PV generators as shown in Section 2.3. The collection grid topology has not been documented but a star configuration has been implemented (see Fig. 2.9). Each group of four PV generators is connected to an intermediate collector from the internal PVPP grid. Notice that one group consists of five PV generators, to sum up to a total of 114 inverters. Then, each intermediate collector is connected to the Point of Common Coupling (PCC). Finally, the connection between the PCC and the transmission grid is implemented through a MV/HV two-winding transformer. To summarize, the LS-PVPP model consists of 114 VSCs, 57 three-winding transformers, 1 two-winding transformer and 71 transmission lines.

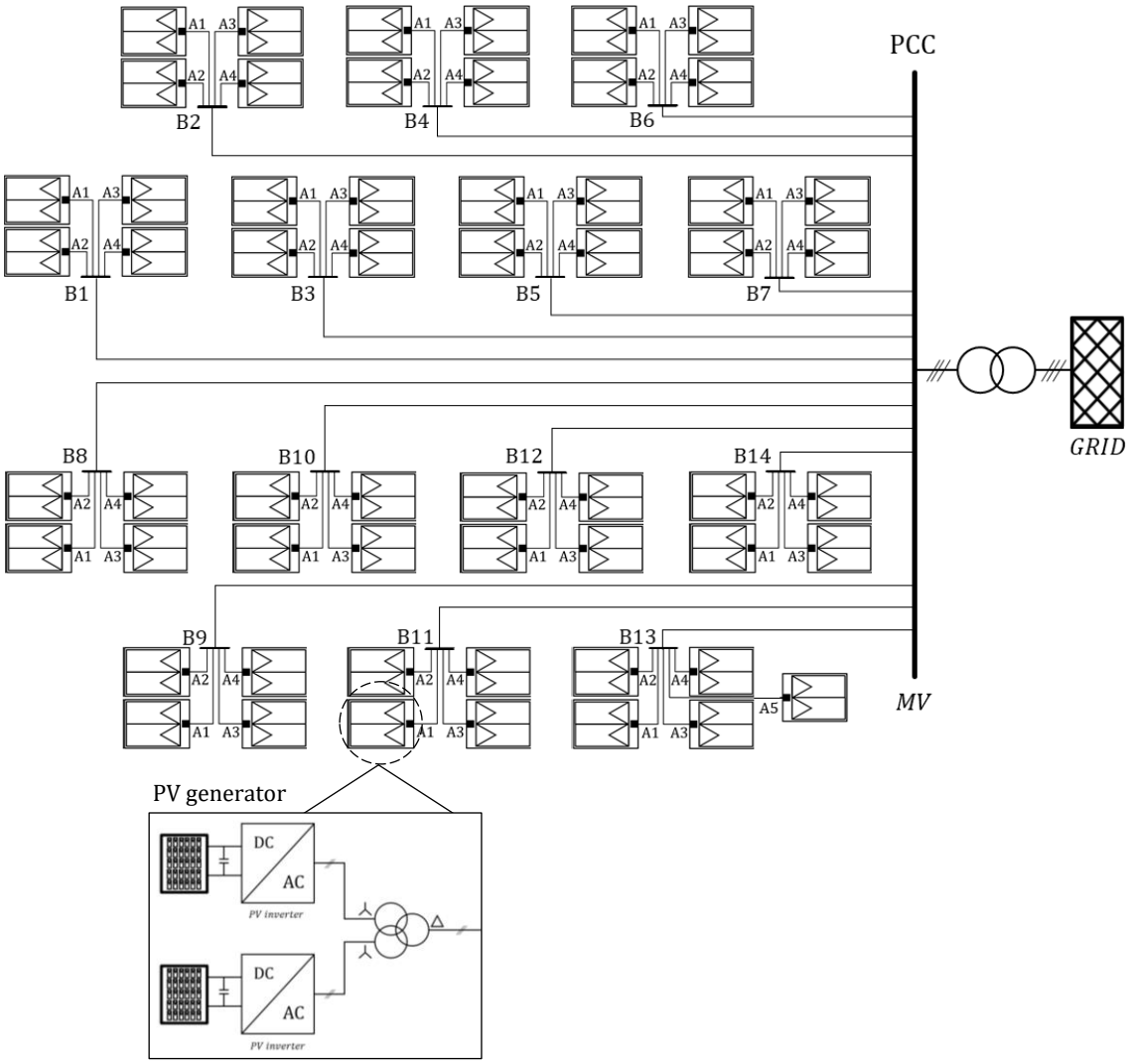


Figure 2.9: LS-PVPP diagram under study

### 2.4.2 Power Plant control

The control of the LS-PVPP is responsible for the regulation of the active and reactive power injected into the electrical system considering the Transmission System Operator (TSO) requirements [54]. Although each PV inverter can perform its own local control according to the active and reactive power references, it is necessary to coordinate the PV inverters to fulfil the desired set-points at the PCC. The active and reactive power are measured at the PCC to assure that the power references are achieved compensating all internal losses. Therefore, the power plant control (PPC) acts as a master to drive all the inverters and it represents the highest level in the overall cascade control system.

The present approach only considers the active power curtailment and the reactive power set-point given by the TSO and it does not take into account any information about the available power.

The proposed active power control system is divided in the controller and the dispatch system as illustrated in Fig. 2.10. The controller is a PI-based that computes the total active power, $P_{ref}^{total}$, that must be generated by all the inverters. Then, the dispatch system distributes the total reference active power among all the controllable inverters. The total $P_{ref}^{total}$ is divided by the total number of PV inverters, $N_{PV_{inv}}$, to obtain $P_{ref,i}$ that is sent to each $i$ inverter. This method is used since all inverters in the plant have the same nominal power, as described in the previous section, and are considered to be fully operational.

The proposed reactive power control follows the same approach as the active power control, as shown in Fig. 2.11. Each PV inverter $i$ receives its local reactive power reference $Q_{ref,i}$.

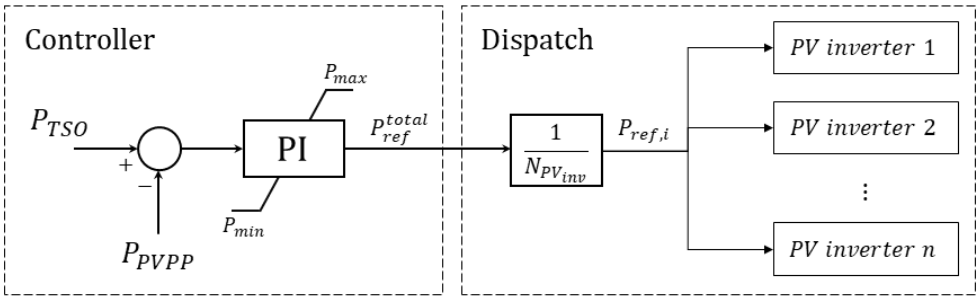


Figure 2.10: Active power plant control

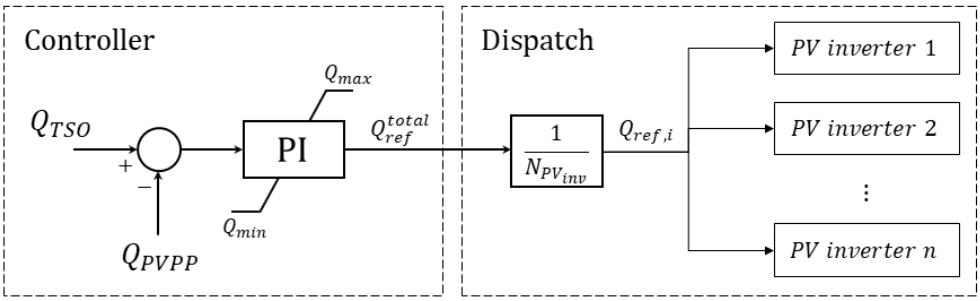


Figure 2.11: Reactive power plant control

The controller design is carried out by the IMC method and is given by

$$F(s) = k_p^{ppc} + \frac{k_i^{ppc}}{s} = \frac{\tau_{oc}}{\tau_{ppc}} + \frac{1}{\tau_{ppc} \cdot s} \tag{2.19}$$

Then comparing both expressions the PI parameters can be stated as

$$k_p^{ppc} = \frac{\tau_{oc}}{\tau_{ppc}} \tag{2.20}$$

$$k_i^{ppc} = \frac{1}{\tau_{ppc}} \tag{2.21}$$

where $\tau_{ppc}$ is the power plant controller time constant.

# Chapter 3

# Simulation results

This chapter describes the simulations performed in OpenModelica and their respective results are presented.

- Case study 1: the PV generator is simulated under different active and reactive power references given to the local control of each PV inverter.
- Case study 2: the LS-PVPP is simulated according to the variations in active and reactive power set-points given by the TSO.

The simulations of both cases studies have been performed using 5 different integration methods, also called solvers, and their respective total simulation times are presented together with some basic numerical statistics. Three basic explicit solvers (Runge-Kutta, fixed step-size, order 4; Heun, fixed step-size, order 2; and Euler, fixed step-size, order 1) and two implicit solvers (DASSL, Backward Differentiation Formula (BDF) method, step-size control, order 1-5; and IDA, BDF method with sparse linear solvers, step-size control, order 1-5) are tested. DASSL is the default solver in OpenModelica. Further characteristics and specifications of each solver can be found in [29].

OpenModelica 1.14.1 has been used to run the simulations on a laptop with an Intel i7-8550U and 8 GB of RAM.

## 3.1 PV generator

The PV generator described in Section 2.3. is tested under variations of the active and reactive power references given to each inverter. Each PV inverter is operated independently and the active and reactive power are measured in the low voltage side. The PV generator is rated at 2 MW and is connected to the internal PVPP medium voltage grid of 20 kV as shown in Fig. 3.1.

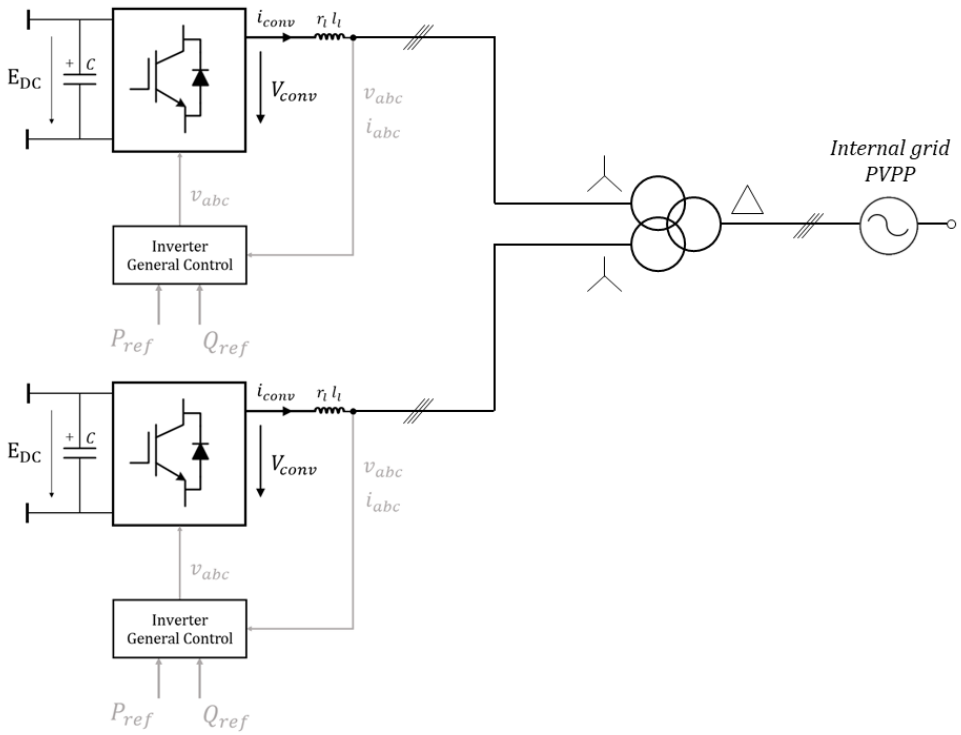


Figure 3.1: PV generator under study

As a reference, the inverter model SMA Sunny Central 900CP XT [55] has been selected and its basic technical data is summarized in Table 3.1. The inverter switching frequency, coupling resistance and inductance have been chosen according to the average value model design. The inverter local control system parameters are calculated following the procedures mentioned in Section 2.2. and are summarized in Table 3.2.

Regarding the calculations to set the PLL parameters:

- The damping ratio is set to $\xi = 0.707$
- The angular velocity of the electrical grid. The grid frequency is fixed to $f = 50$ Hz, therefore $\omega_e = 2 \cdot \pi \cdot f = 314.16 \frac{\text{rad}}{\text{s}}$
- The admitted peak voltage. If the low voltage grid is in star connection and its voltage is the same as the inverter output AC voltage, then $E_m = \frac{405}{\sqrt{3}} \cdot \sqrt{2} = 330.68$ V

Concerning the PV generator modelling, according to the manufacturer [19] if there is a neutral-point terminal on the low voltage side, this neutral point terminal must not be grounded or connected. However, for the numerical stability of the simulation, it has been grounded.

Table 3.1: Inverter parameters. DC side as a voltage source

| Parameters | Symbol | Value | Units |
|---|---|---|---|
| Inverter nominal AC power | $S$ | 900 | kVA |
| Inverter nominal DC voltage | $E_{DC}$ | 722 | V |
| Inverter nominal AC voltage (phase-to-phase) | $V_{RMS}$ | 405 | V |
| Inverter switching frequency | $f_{sw}$ | 10 | kHz |
| Coupling resistance | $r_l$ | 5.55 | mΩ |
| Coupling inductance | $l_l$ | 60 | $\mu$H |

Table 3.2: Inverter local control parameters

| Component | Parameters | Value | Units |
|---|---|---|---|
| PLL | $k_p^{PLL}$ | 1.34 | rad/Vs |
| | $\tau_{PLL}$ | 4.5 | ms |
| Inner current controller | $k_p^{icc}$ | 0.06 | H/s |
| | $k_i^{icc}$ | 5.55 | Ω/s |
| | $\tau_{icc}$ | 1 | ms |
| Outer controller | $k_p^{oc}$ | 0.0002016 | $V^{-1}$ |
| | $k_i^{oc}$ | 0.2016 | $V^{-1} \cdot s^{-1}$ |
| | $\tau_{oc}$ | 10 | ms |

### 3.1.1 Active and reactive power dynamic response

In order to test the inverter response, changes in active and reactive power references are applied to each single inverter as described in Table 3.3.

Reference and measured values of active and reactive power are illustrated in Fig. 3.2 and Fig. 3.3. These power values change accordingly to the reference values described in Table 3.3. The output current and the voltage in the *abc* frame of a single inverter are plotted in Fig. 3.4 and Fig. 3.5. The current injected to the internal PVPP medium voltage grid and its voltage in the *abc* frame are illustrated in Fig. 3.6 and Fig. 3.7.

Table 3.3: Active and reactive power references

| Time [s] | Active power reference [kW] | Reactive power reference [kvar] |
|---|---|---|
| 0 | 600 | 0 |
| 0.4 | 200 | 0 |
| 0.5 | 200 | -300 |
| 1 | 900 | -500 |
| 1.5 | 500 | 0 |

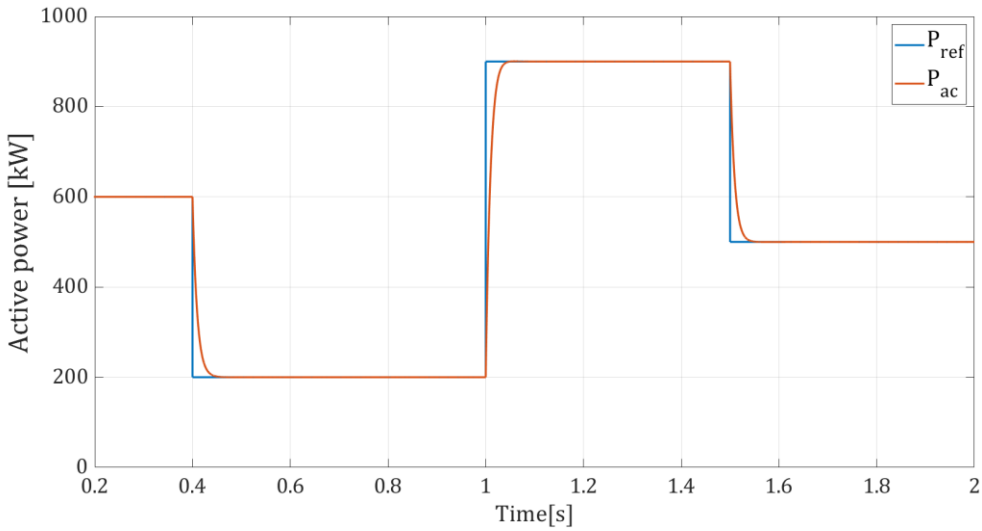


Figure 3.2: Reference and measured active power injected to the grid

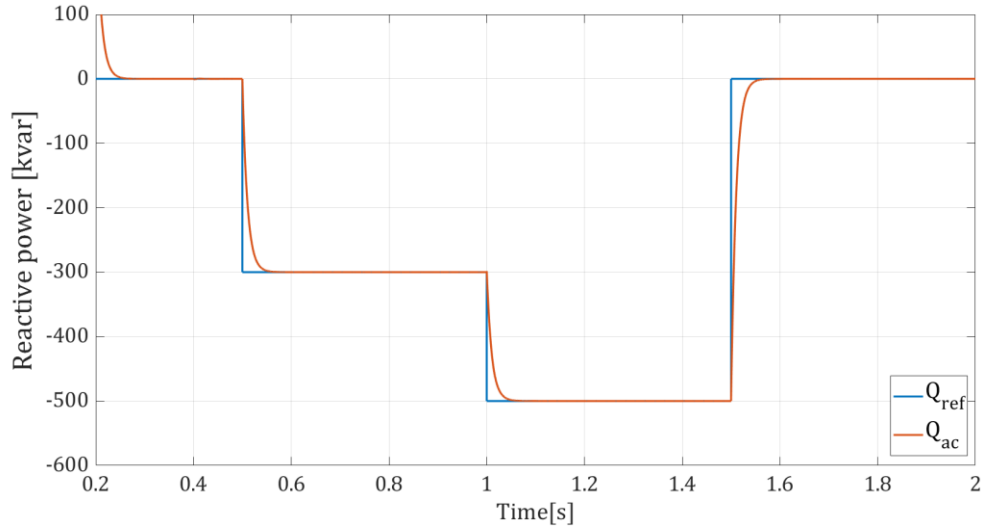


Figure 3.3: Reference and measured reactive power injected to the grid

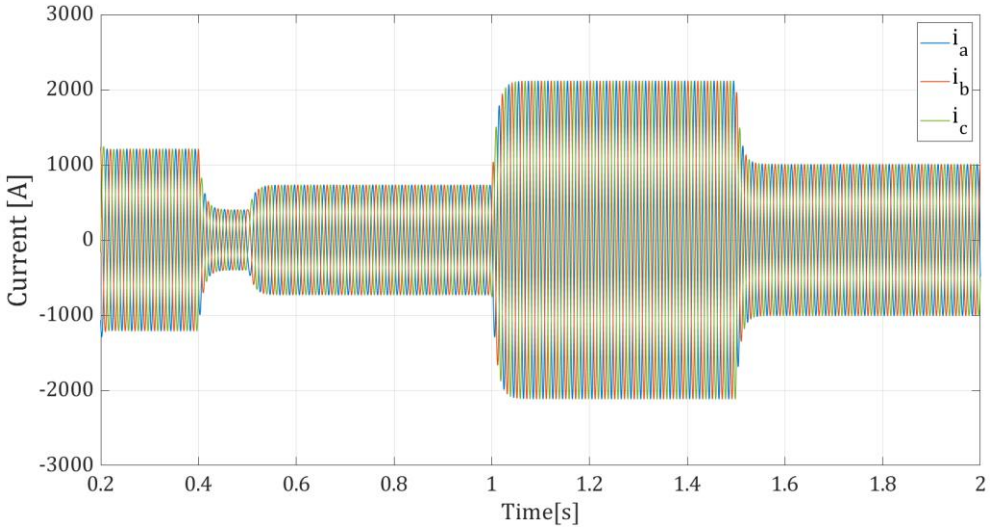


Figure 3.4: Inverter output current in the low voltage side in *abc* frame

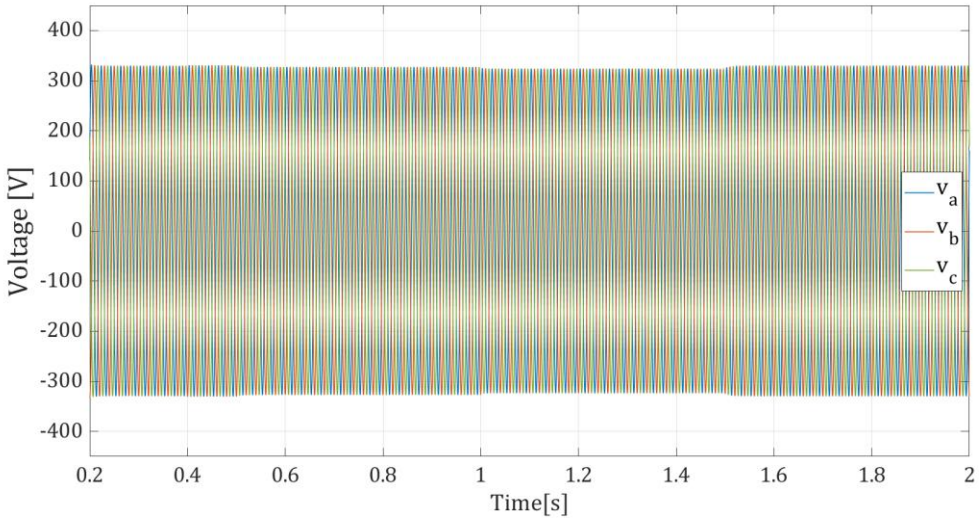


Figure 3.5: Inverter voltage in *abc* frame

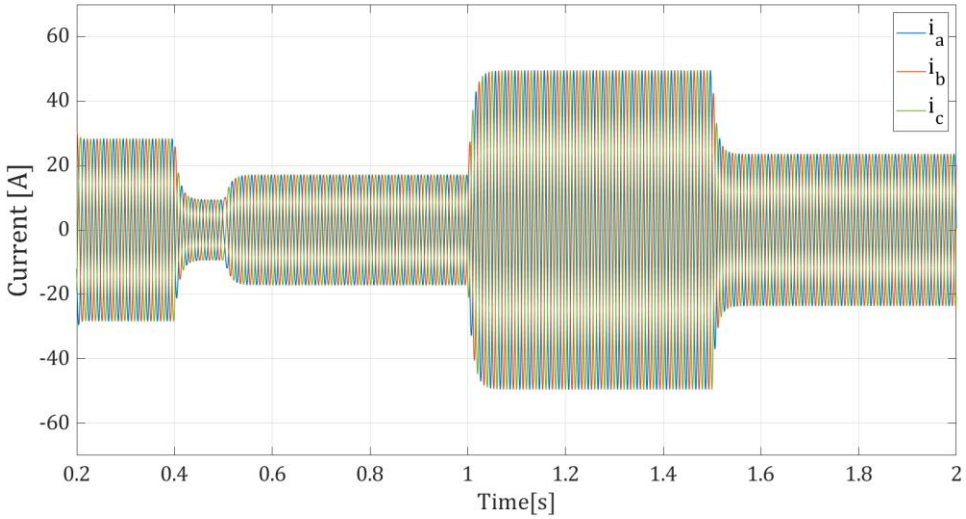


Figure 3.6: PV generator output current injected at the medium voltage side in *abc* frame

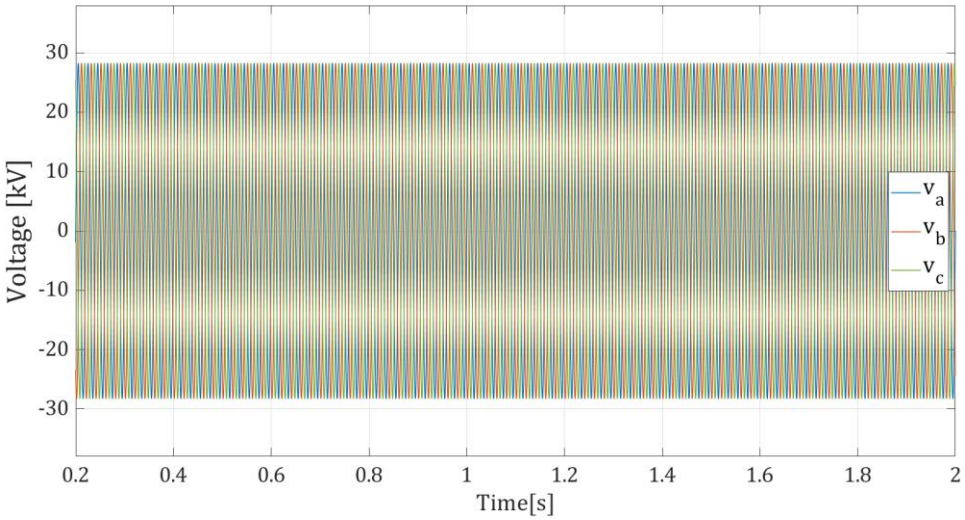


Figure 3.7: Internal PVPP grid voltage in *abc* frame

### 3.1.2 Integration methods comparison and numerical statistics

The model statistics after passing the front-end and creating the data structures used by the back-end are:

- Number of equations: 1516
- Number of variables: 1516
- Number of states: 20

Table 3.4: Integration methods and total simulation times comparison of the PV generator model

| Integration method | Step-size | Tolerance | Time | Total simulation time |
|---|---|---|---|---|
| Euler | 100 $\mu s$ | $1 \cdot 10^{-4}$ | 2 s | 1.47 s |
| Runge-Kutta | 100 $\mu s$ | $1 \cdot 10^{-4}$ | 2 s | 1.84 s |
| Heun | 100 $\mu s$ | $1 \cdot 10^{-4}$ | 2 s | 1.42 s |
| DASSL | 100 $\mu s$ | $1 \cdot 10^{-4}$ | 2 s | 2.03 s |
| IDA | 100 $\mu s$ | $1 \cdot 10^{-4}$ | 2 s | 2.23 s |

## 3.2 Large Scale Photovoltaic Power Plant

The inverter parameters are set as in Section 3.1. The LS-PVPP model under analysis is the one presented in Section 2.4. The PPC parameters are summarized in Table 3.5. As the PPC represents the highest level in the cascade control system, its time constant has to be the highest. The time constant should be set according to the grid code established by the German Association of Energy and Water Industry (BDEW). However, due to the simplification of the PPC and simulation duration issues, is set to 100 ms, ten times higher than the lower system, in this case, the local active and reactive power control of each inverter.

Table 3.5: Power plant control parameters

| Component | Parameters | Value | Units |
|---|---|---|---|
| Power Plant Control | $k_p^{ppc}$ | 0.1 | p.u. |
| | $k_i^{ppc}$ | 10 | $s^{-1}$ |
| | $\tau_{ppc}$ | 100 | ms |
| | $N_{PV_{inv}}$ | 114 | inverters |

According to [42] and the data provided by SMA the Dy1y1 three-winding transformers parameters are summarized in Table 3.6.

Table 3.6: Three-winding transformer data

| $V_p$ [kV] | $V_s$ [kV] | $V_t$ [kV] | $S_n$ [MVA] | r + jx [p. u. ] |
|---|---|---|---|---|
| 20 | 0.405 | 0.405 | 2 (Primary) | $0.0077 + j0.051$ |
| | | | 1 (Secondary) | $0.0089 + j0.051$ |
| | | | 1 (Tertiary) | $0.0089 + j0.051$ |

The two-winding MV/HV transformer parameters are described in Table 3.7. The vector group of this transformer is Yy. Both sides of the transformer are grounded.

Table 3.7: Two-winding transformer data

| $V_p$ [kV] | $V_s$ [kV] | $S_n$ [MVA] | r + jx [p. u. ] |
|---|---|---|---|
| 110 | 20 | 128 | $0.003 + j0.116$ |

The plant is assumed to be connected to a transmission grid with the characteristics described in Table 3.8 according to [57].

Table 3.8: Equivalent grid data

| Voltage [kV] | Short circuit power [MVA] | Short circuit ratio (X/R) |
|---|---|---|
| 110 | 6000 | 10 |

Considering the 214 ha of extension of the Templin Photovoltaic Power Plant and the star collection grid configuration described in Section 2.4, the cables length and impedances (according to Nexans [58]) are described in Table 3.9 and Table 3.10. The capacitance effect has been neglected due to solver issues and simulation execution. Table 3.9 summarizes the impedance values of the lines that connect the PV generator to its respective intermediate collector, and Table 3.10 the impedance values of the lines that connect each collector to the PCC.

Table 3.9: Transmission lines data from PV generator to intermediate collector for n = 1 to 14

| Node 1 | Node 2 | Line length [km] | Line R[Ω] | Line X[mΩ] |
|---|---|---|---|---|
| A1 | Bn | 0.2 | 0.026 | 0.0672 |
| A2 | Bn | 0.2 | 0.026 | 0.0672 |
| A3 | Bn | 0.2 | 0.026 | 0.0672 |
| A4 | Bn | 0.2 | 0.026 | 0.0672 |
| A5 | Bn | 0.2 | 0.026 | 0.0672 |

Table 3.10: Transmission line data from intermediate collector to the PCC

| Node 1 | Node 2 | Line length [km] | Line R[Ω] | Line X[mΩ] |
|---|---|---|---|---|
| B1, B8 | PCC | 2.2 | 0.286 | 0.739 |
| B2, B9 | PCC | 2 | 0.26 | 0.672 |
| B3, B10 | PCC | 1.8 | 0.234 | 0.605 |
| B4, B11 | PCC | 1.6 | 0.208 | 0.538 |
| B5, B12 | PCC | 1.4 | 0.182 | 0.469 |
| B6, B13 | PCC | 1.2 | 0.156 | 0.403 |
| B7, B14 | PCC | 1 | 0.13 | 0.336 |

### 3.2.1 Active and reactive power dynamic response

In order to test the power plant response, changes in active and reactive power set-points according to the TSO are described in Table 3.11. The set-points and the measured values at the PCC of the active and reactive power are illustrated in Fig. 3.8 and Fig. 3.9. These power values change accordingly to the reference values.

The output current and the voltage of a single inverter in the low voltage side in the *abc* frame are plotted in Fig. 3.10 and Fig. 3.11. The output current of a single PV generator in the *abc* frame is illustrated in Fig. 3.12. The measured voltage in the PV generator – internal PVPP grid connection in the *abc* frame is plotted in Fig. 3.13. Finally, the measured current and voltage at the PCC in the *abc* frame are shown in Fig. 3.14 and Fig. 3.15.

Table 3.11: TSO active and reactive power set-points

| Time [s] | Active power reference [MW] | Reactive power reference [Mvar] |
|---|---|---|
| 0 | 70 | 0 |
| 0.4 | 70 | -25 |
| 0.6 | 100 | -25 |
| 1 | 100 | 0 |
| 1.4 | 60 | 0 |
| 1.5 | 60 | -50 |

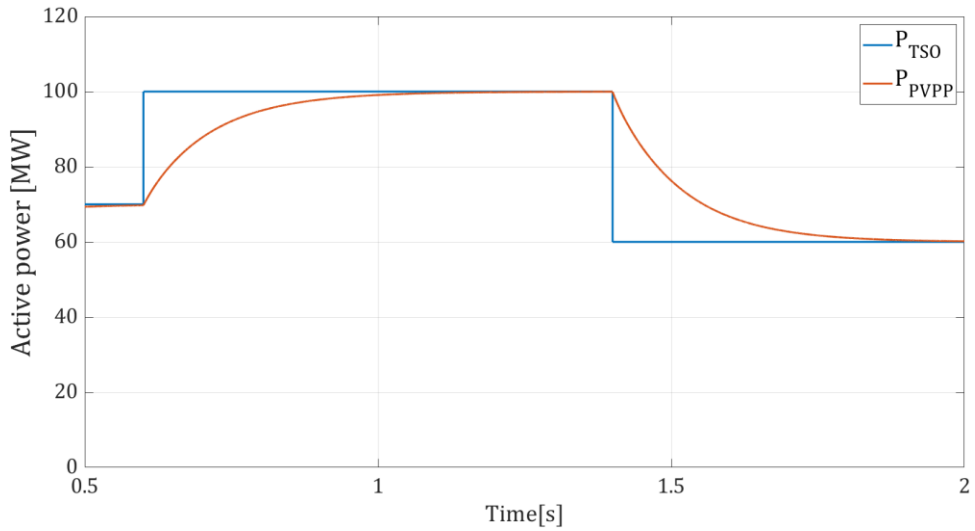


Figure 3.8: Active power response

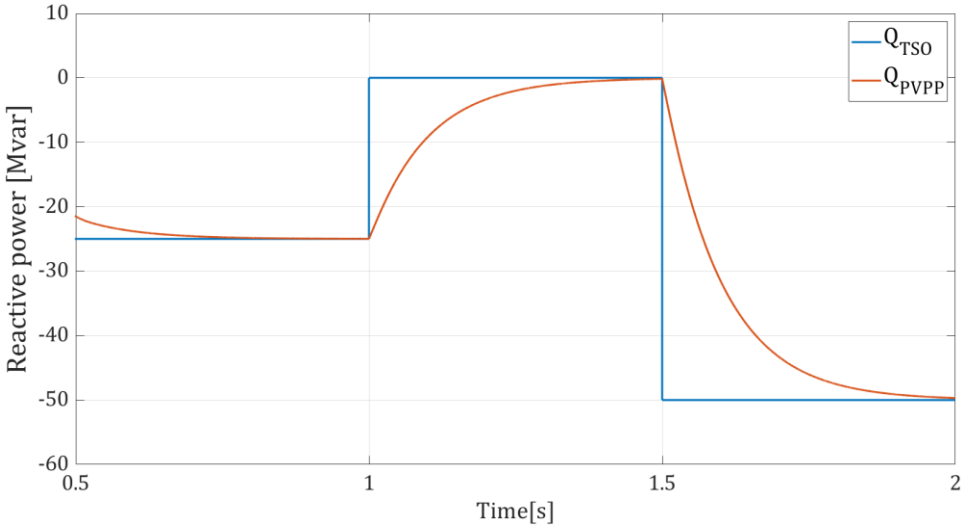


Figure 3.9: Reactive power response

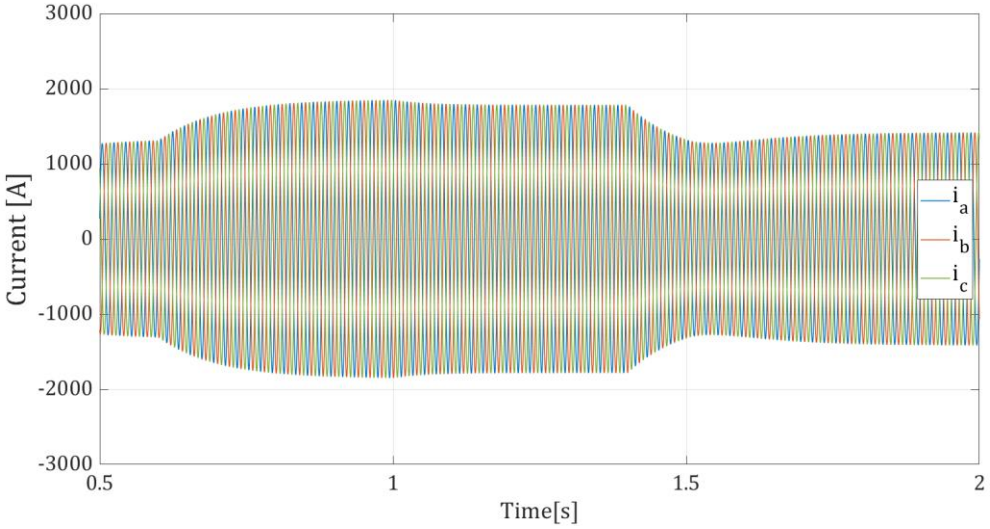


Figure 3.10: Single inverter output current in *abc* frame

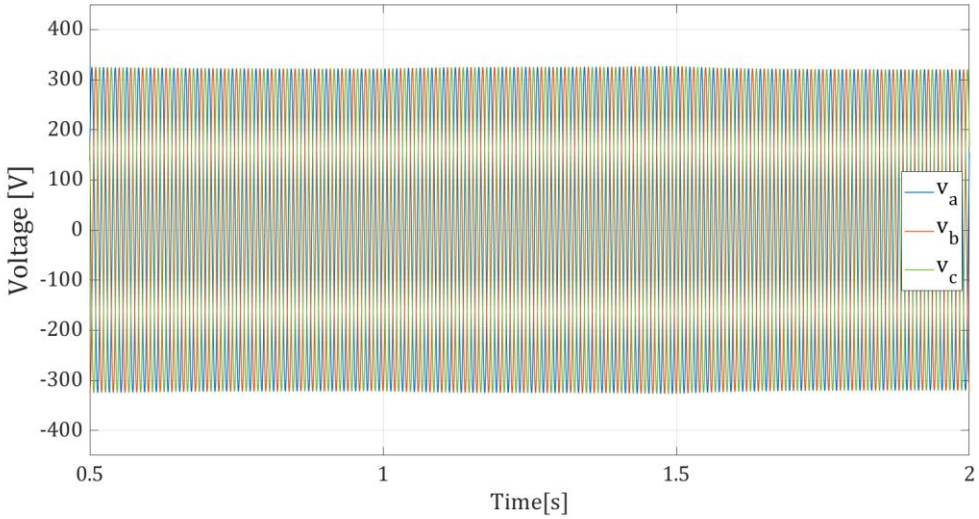


Figure 3.11: Single inverter voltage in *abc* frame

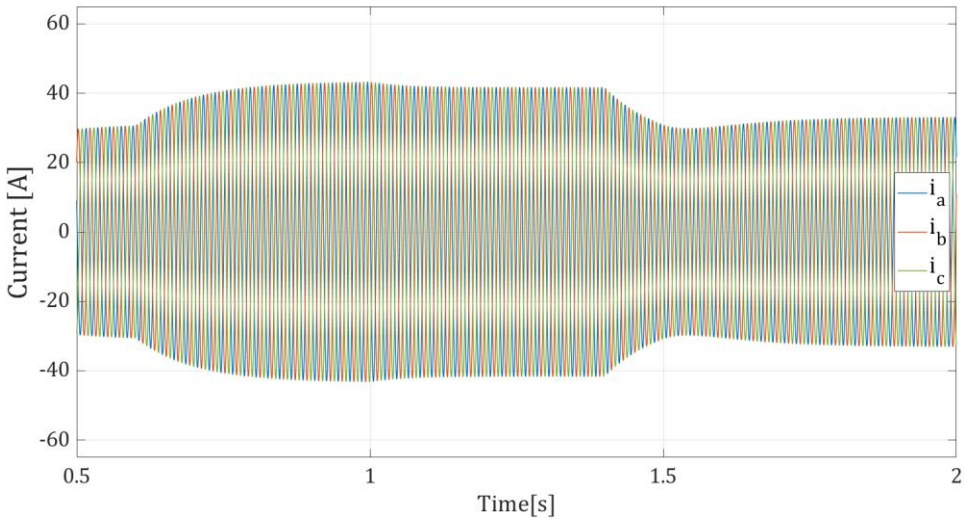


Figure 3.12: Single PV generator output current in *abc* frame

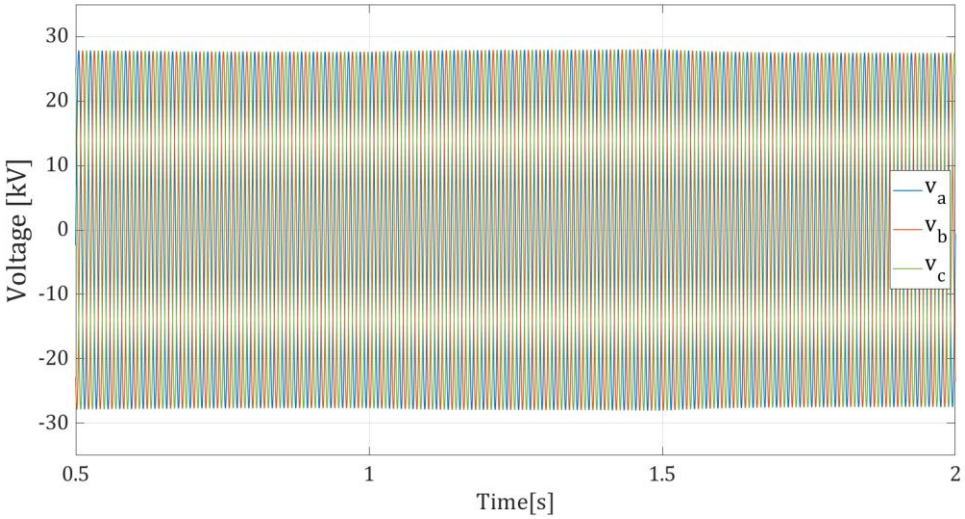


Figure 3.13: Measured voltage in the PV generator – internal PVPP grid connection in *abc* frame

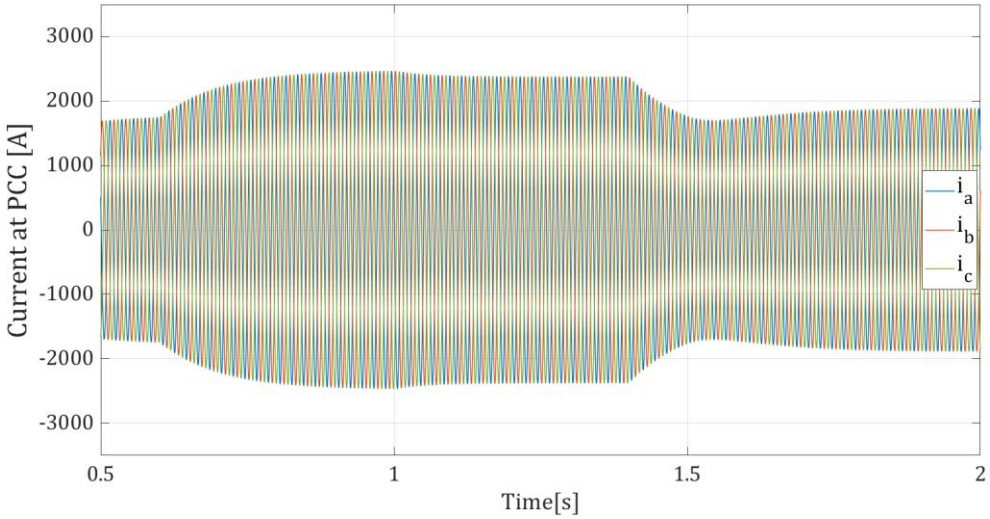


Figure 3.14: Measured current at the PCC

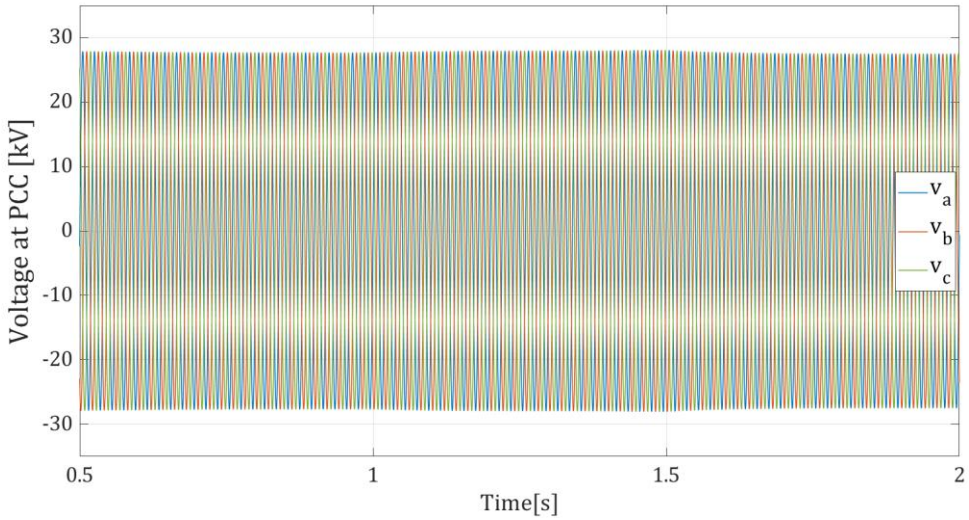


Figure 3.15: Measured voltage at the PCC

### 3.2.2 Integration methods comparison and numerical statistics

The model statistics after passing the front-end and creating the data structures used by the back-end are:

- Number of equations: 75458
- Number of variables: 75458
- Number of states: 1030

Therefore, the model can be classified as large-scale as defined in [25]. Due to performance issues and problems encountered that will be mentioned in the discussion section, the simulation has been carried out without implementing the inductances in the transformers. The model compilation takes an average of 40 minutes from the total simulation time. The total simulation time by using each integration method is summarized in Table 3.12.

Table 3.12: Integration methods and total simulation times comparison of the LS-PVPP model

| Integration method | Step-size | Tolerance | Time | Total simulation time |
|---|---|---|---|---|
| Euler | 100 $\mu s$ | $1 \cdot 10^{-4}$ | 2 s | 1 h 08 min |
| Runge-Kutta | 100 $\mu s$ | $1 \cdot 10^{-4}$ | 2 s | 2 h 13 min |
| Heun | 100 $\mu s$ | $1 \cdot 10^{-4}$ | 2 s | 2 h 01 min |
| DASSL | 100 $\mu s$ | $1 \cdot 10^{-4}$ | 2 s | Stopped after 20 h |
| IDA | 100 $\mu s$ | $1 \cdot 10^{-4}$ | 2 s | Stopped after 20 h |

# Chapter 4

# Discussion

In this chapter, the dynamic response of the PV generator and the LS-PVPP under the active and reactive power step references is analysed. The objective is to determine whether the time response of each controller satisfies the specifications set in the design. Then, briefly discuss if the inverter performance conforms to the manufacturer specifications.

Finally, a section concerning troubleshooting and numerical issues, comparison between the different integration methods used, problems encountered during the modelling and simulation of the systems is presented along with an analysis regarding TLM and parallelization capabilities.

## 4.1 Case study 1

As expected, the active and reactive power response match the first order dynamics. Then, it must be verified that both responses settle to 98 % of its reference value within $4 \cdot \tau_{oc}$ s according to the first order systems response criterion [59]. Approximately, according to the detailed active and reactive power response of a single inverter illustrated in Fig. 4.1:

- Active power: 99.5 %
- Reactive power: 98 %

Can be considered that both responses fulfil the set time constant specifications. However, if a more accurate response is required the PI parameters can be re-tuned manually. The trial-and-error approach is also a valid method even though could be time-consuming.

Another issue to consider is that in the controller design process the $v_z^q$ has been considered constant. However, in reality this is not the case, since there are variations even though they are quite slight.

On the other hand, regarding the inverter AC generated current, according to [55] the maximum output current is 1411 A. The inverter rated power is 990 kVA even though the parameters have been set according to the nominal AC power of 900 kVA.

Therefore, the maximum admitted peak value is $1411 \cdot \sqrt{2} = 1995.45$ A. Between instant $t = 1$ and $t = 1.5$ the apparent power injected is

$$S = \sqrt{P^2 + Q^2} = 1029.5 \text{ kVA} \tag{4.1}$$

The generated current (see Fig. 4.2) is slightly higher than the maximum output current because the power reference values are also slightly higher than the 990 kVA rated power.

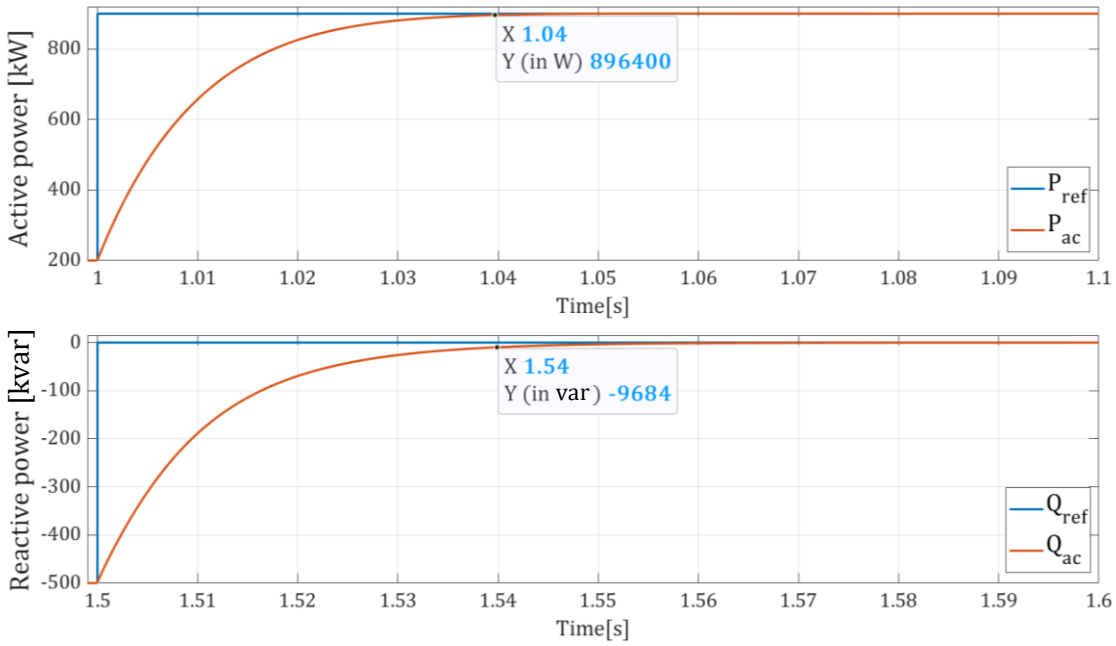


Figure 4.1: Active and reactive power response of a single inverter

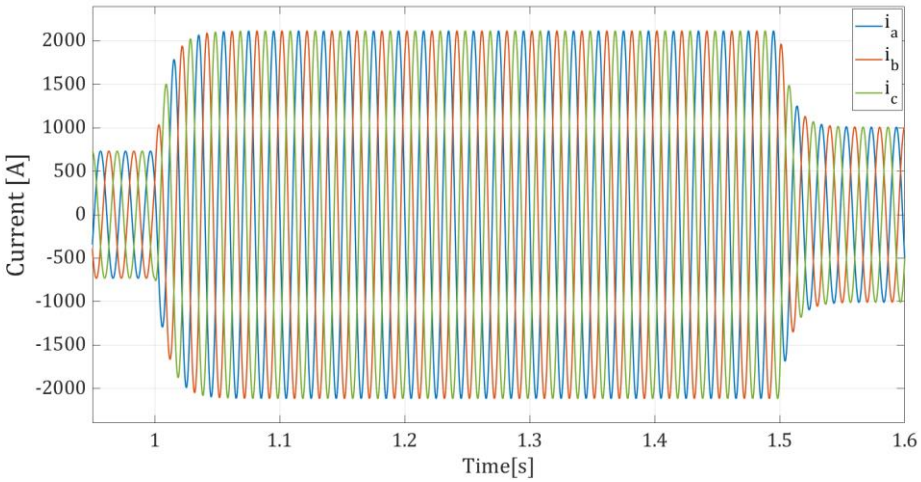


Figure 4.2: Single inverter output current

## 4.2 Case study 2

The results show a good response and the capacity to perform independent active and reactive power control.

The same concept as in case study 1 is considered. Both responses match the first order dynamics. Then, it must be verified that both responses settle to 98 % of its reference value within $4 \cdot \tau_{ppc}$ s according to the first order systems response criterion [59]. According to the active and reactive power measured at the PCC as plotted in Fig. 4.3:

- Active power: 97 %
- Reactive power: 98.25 %

Therefore, can be considered that the implemented power plant control fulfils the time response specifications.

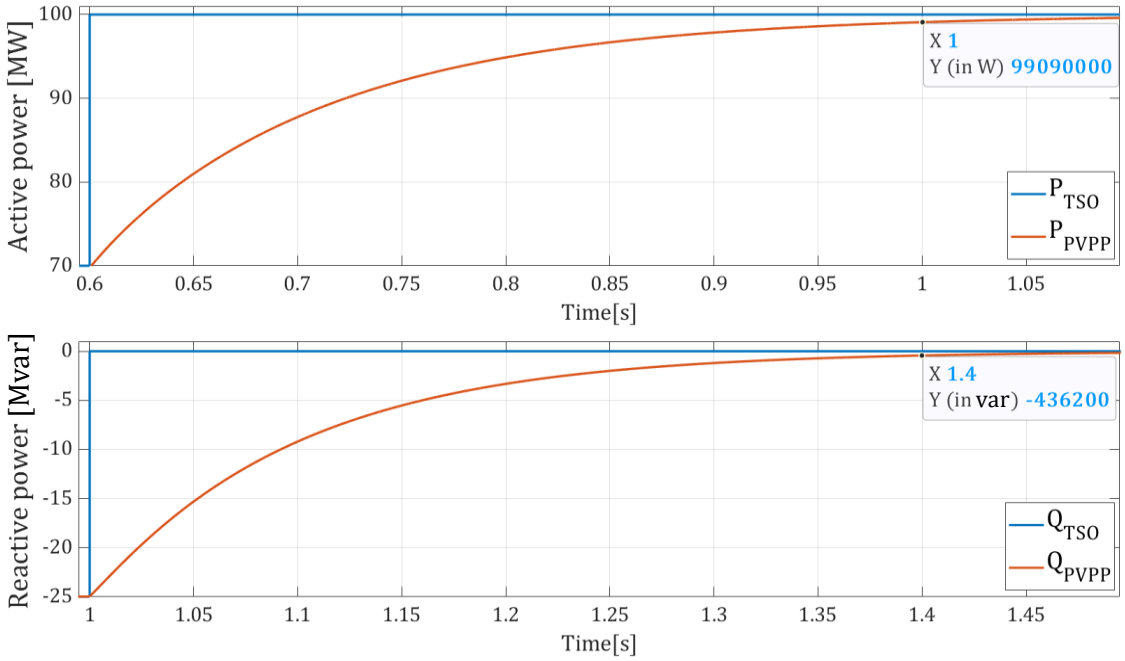


Figure 4.3: Active and reactive power response

## 4.3 Troubleshooting and numerical issues

*Modelling*

First, regarding the LS-PVPP model, if the transmission lines that connect the *B* nodes to the PCC converge directly to the PCC electrical three-phase plug, the linear system becomes

singular and cannot be solved. Therefore, the lines have been connected to four different plugs and later on connected to the PCC.

Moreover, regarding the same issue, some problems and errors have been encountered when using the positive and negative electrical three-phase plugs. For example, positive-positive or negative-negative connections. To avoid these errors, the neutral plug has been used in the PV generator – three-winding transformer, the *B* nodes – transmission lines, and the PCC plug connections.

As mentioned in Section 3.1, the low voltage windings of the three-phase must be grounded to execute successfully the simulation.

*Solvers*

In the PV generator model, the simulation times using Euler solver (the fastest) and the IDA solver (the slowest) differ by 50%. The explicit solvers are faster than the implicit ones.

The main reason why the explicit solvers are at least 10 times faster than the implicit ones in the simulation of the LS-PVPP model is that they avoid computing the dense Jacobian. In [28] a similar issue is more deeply discussed. Therefore, it may not be optimal the use of implicit ODE solvers for these types of systems. In the PV generator model simulation, the Jacobian is not as large and dense, and consequently, the simulation times between using explicit and implicit integration methods are considerable similar.

The slow simulation may be also caused by numerical instabilities in the significantly stiff equation system formed at the PCC. Even though the system can be simulated, it remains close to numerical singularity and it becomes hard to solve for the solver. In the LS-PVPP not only the large number of equations (75458) and states (1030) but the structure of this type of systems, where all the PV generators are connected to the same point (the PCC) has probably a considerable impact in the simulation time. Moreover, the large number of resistances and inductances can lead to a lot of redundant equations. However, the redundancy between these components could be exploited to speed up the compilation [32].

Consider that only 2 seconds simulations are performed. Even so, at least one hour is required to simulate the LS-PVPP model using the Euler solver (fastest method). Furthermore, the type of models analysed are more complex in real industry cases. For example, in the LS-PVPP model, only by adding the inductances in the transformers, and implementing PI section transmission lines the number of equations and states increase to 88310 and 1441, respectively. Then, the system becomes much stiff and cannot be solved.

For that reason, new solving methods and approaches and/or different ways of modelling should be researched.

On the other hand, the precision of the simulations results is not affected by the type of solver used, probably because the step-size is set to 100 $\mu$s and the work is conducted with 20 ms period waves.

*DAE mode*

Regarding the DAE mode exposed in Section 2.1.1, it has been considered as a possibility to improve the simulation performance and to reduce the simulation time. However, both the LS-PVPP and the PV generator models have been tested under the DAE mode but it seems like some function *intMod* does not work yet and the simulation cannot be executed. Even though the DAE mode is operational, it does not have the same coverage as regular Ordinary Differential Equations (ODE) mode currently. DAE mode should be better for big systems with many nonlinear loops even though it does not run models that do not run under ODE mode since it will have the same problems with some issues such as dynamic differential index.

*Index reduction*

In general terms, index reduction can be stated as the following: if algebraic constraints are put in two states (e.g. setting them equal) index reduction takes place because two states must be independent of each other to be states. If they are algebraically coupled one of them has to be a regular algebraic variable and not a state for the whole system to make sense.

An index reduction example from the PV generator test model where (see Fig. 4.4): *PV_unit* is the PV generator that consists of two PV inverters and a three-winding transformer; *T1* is the Dy1y1 three-winding transformer; *L1* is the inductance in the medium voltage side of the transformer in delta connection; *Lc* is the VSC coupling inductance; *n12* and *n13* are the ratios of the primary voltage to the secondary and tertiary.

For each phase, the same process is carried out even though only one is exposed.

```
Index Reduction neccessary!
MSS subsets:
 205
 204
 203

###############--MSSS--###############
Indices of constraint equations: 203

------------------203------------------
Constraint equation to be differentiated:
0.0 = PV_unit.T1.L1.inductor[1].i + PV_unit.VSC1.Lc.inductor[1].i / PV_unit.T1.core.n12 + PV_unit.VSC2.Lc.inductor[1].i / PV_unit.T1.core.n13
Differentiated equation:
0.0 = der(PV_unit.T1.L1.inductor[1].i) + der(PV_unit.VSC1.Lc.inductor[1].i) / PV_unit.T1.core.n12 + der(PV_unit.VSC2.Lc.inductor[1].i) / PV_unit.T1.core.n13
```

Figure 4.4: Index reduction example in OMC

The reason why the LS-PVPP model simulation with the inductances both in the three-winding and two-winding transformers cannot be executed may be due to some problems with index reduction which lead to an assertion at initialization.

There are constraints due to the connection topology. In this case, in the star connection of the low voltage windings of the three-winding transformers. If this is not recognized by the back-end, then sooner or later some singular equations will be found, which seems to be the case. In

this context, tests have shown that exactly the same model implemented with a Yy transformer fails to execute and, on the contrary, if a Dd structure is implemented, the simulation is able to run.

In [60] there is ongoing work to solve this issue. In [61] a similar numerical issue regarding index reduction is deeply discussed. Notice that OpenModelica is in constant development.

However, a deep understanding of the back-end process is required to understand most of the processes carried out to understand how simulations are executed [62].

*Initialization*

To be able to solve the models is important to provide as many sensible start values as possible to make the initialization stable. Since there is index reduction going on, all of the states in the system need to be initialized properly. Otherwise, there may be an initialization problem. However, an overdetermination in the start values can lead to an inconsistent initialization problem.

The slow simulation times could also be caused by possible instabilities in the initialization problem, apart from the solver's issues mentioned in the previous subsection.

Regarding the LS-PVPP model simulation, if no start values are provided, the OMC needs to assume fixed start values for 342 variables (see Fig. 4.5), which could lead to an assert at initialization and a following simulation execution failure. However, by setting sensible start values to the current flowing through the primary winding of the three-winding transformers, the assumed start values decrease to 171, making the initialization problem simpler.

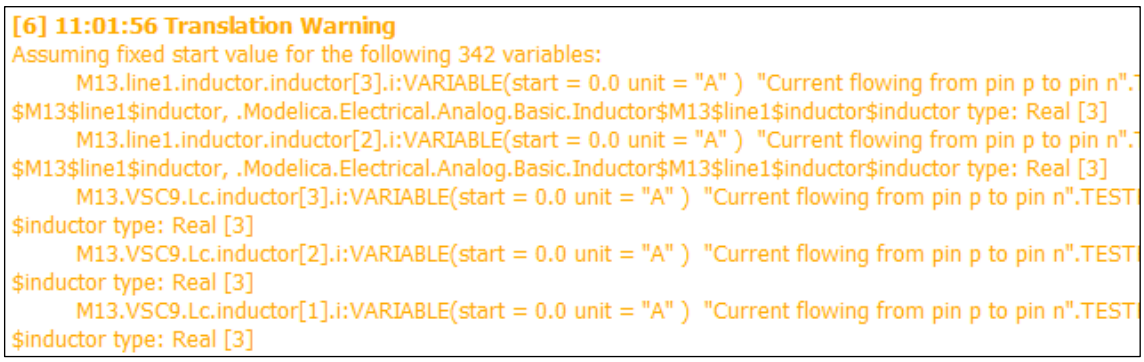


Figure 4.5: Assuming fixed start values initialization warning

The LS-PVPP model with inductances in the three-winding and two-winding transformers breaks because it fails at initialization even though sensible start values are set: *solving the non-linear system fails and the simulation terminates by an assertion at initialization.* Currently,

there is ongoing work to solve this issue. Probably this could be also solved by some form of diode implementation.

If the LS-PVPP model is simulated implementing PI section lines and the complete three-winding and two-winding transformers models, the unfixed start variables increase to 753 (see Fig. 4.6). Therefore, the system initialization becomes much instable.

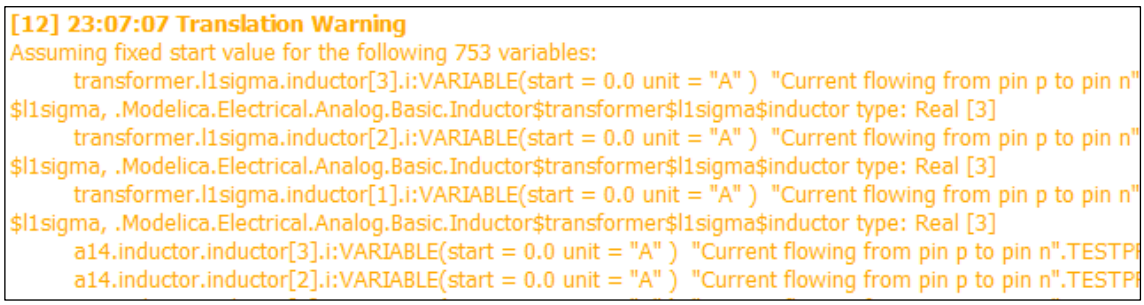


Figure 4.6: Assuming fixed start values initialization warning 2

*TLM and Parallelization*

First, regarding the TLM approach, it may be unsuitable for very stiff systems such as large electrical systems with a high number of resistors, inductances or capacitors connected to each other [35]. Moreover, TLM may not be the optimal parallelization approach because each model should be adapted to this way of modelling.

The HPCOM parallelization implementation [40, 42, 62], which is still under construction and may not be fully operational, has been tested in the simulation of the PV generator model described in Section 3.1. If the same method is tested in the LS-PVPP model, the simulation execution fails. It is mostly an automatic implementation that is enabled by the flag *-hpcom* given to the OMC. Basically, the method consists in dividing the model into several independent parts and identifying their relationships among each other. The representation of these parts is called a task graph. These tasks are created based on the BLT structure, derived from the right-hand side of the model equations.

First, without applying any parallelization method, the task graph generated from the ODE system in the PV generator simulation is shown in Fig. 4.7. Can be noticed that there is an uneven distribution of the tasks and a central element, one big torn non-linear system, acts as a bottleneck during the solving of the model.

Then, the PV generator model is tested under the HPCOM implementation. In Fig. 4.8. and Fig. 4.9 is shown that the task graph has the same structure than the task graph generated without applying any parallelization method, the same big torn non-linear system appears. Therefore, any speed-up is achieved. Moreover, if this torn non-linear system is partitioned, the simulation execution fails.

Finally, even though the task graph parallelization approach is able to reduce the simulation time for some models [40], it may not be the optimal method to address the studied power system models, which have a high number of strongly connected components (see Fig. 4.10). However, consider again that OpenModelica parallelization capabilities are in constant development.

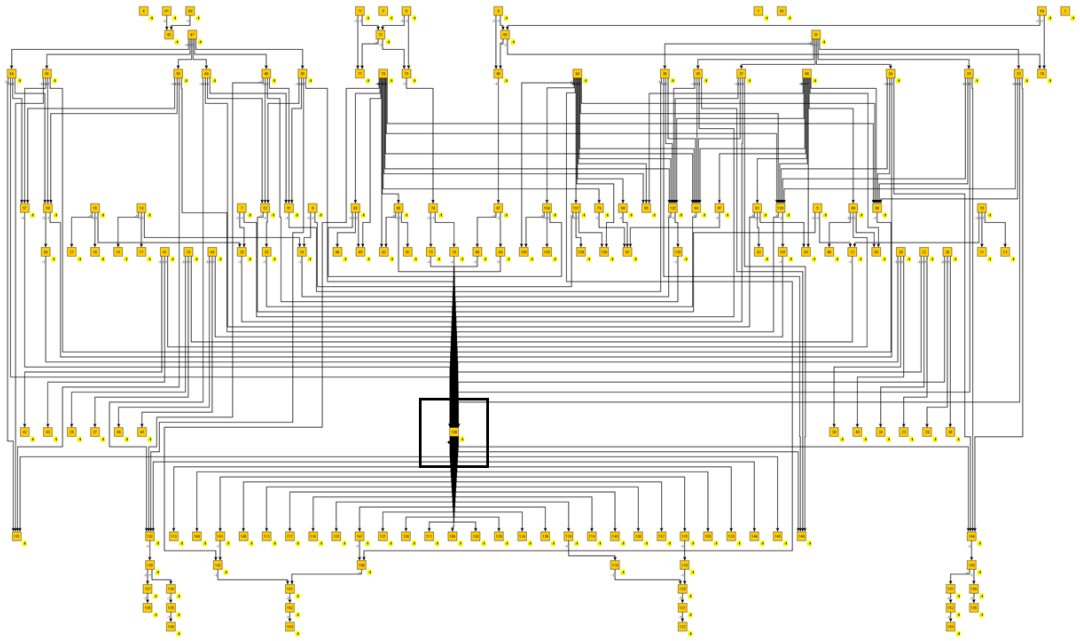

Figure 4.7: Task graph generated in the PV generator model simulation

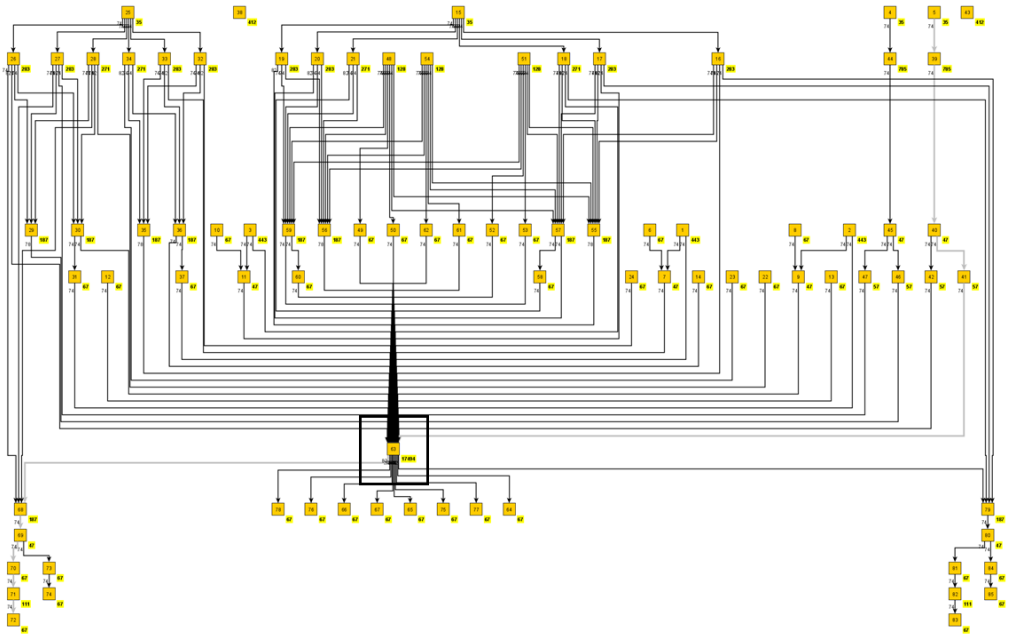

Figure 4.8: Task graph generated in the PV generator model simulation under HPCOM-Module usage

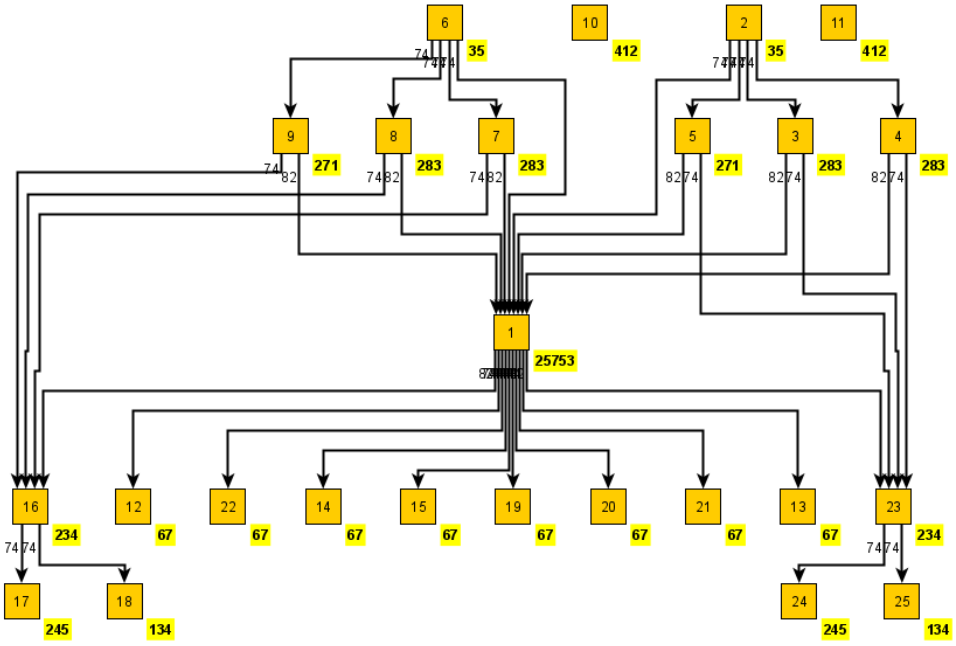


Figure 4.9: Merged task graph schedule generated under HPCOM-Module usage

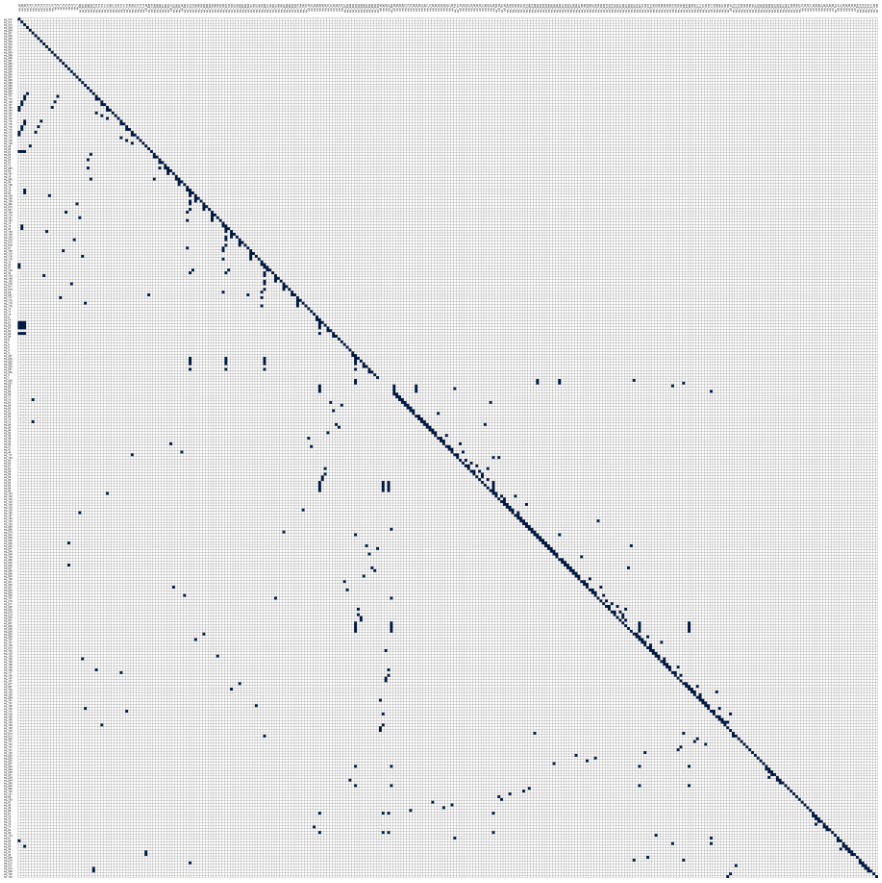

Figure 4.10: BLT representation of the PV generator model

# Chapter 5

# Conclusions and Future Research

This thesis has introduced the principles of a PV inverter based on the VSC, its local dynamic control, and its integration in a LS-PVPP. These principles enabled the design and simulation of a PV generator and a LS-PVPP models. The PV generator model has been tested under different active and reactive power reference values given to each inverter. The LS-PVPP model has been tested under variations in the active and reactive power set-points according to the TSO requirements. The results show an optimal dynamic response of both models and the capacity to perform independent active and reactive power controls.

Several difficulties have come across during the simulation and operation of large-scale models. Besides, runtime compilation and simulation are slow in large-models. OpenModelica performance in the studied power system models may not be still competitive with the domain-specific tools. However, consider OpenModelica limited resources compared to conventional commercial power systems software.

Regarding the power system models of study, task graph-based parallelization approach may not be a suitable method to speed up simulations.

Further research should implement the PV inverter considering the PV array to study the dynamic behaviour of the LS-PVPP under different solar irradiance conditions. Also, test the performance of the inverters under asymmetrical loads. Moreover, improve the LS-PVPP control considering communication delays for PPC and frequency and voltage support to comply with the grid codes. Besides, future studies should include PI section transmission lines that consider the capacitive effect of real cables and a more realistic electrical grid model.

As an outcome, OpenModelica is a promising tool for power system modelling and simulation even though existing barriers and difficulties must be overcome.

# Chapter 6

# Environmental impact

Photovoltaic power deployment is expanding rapidly, especially large installations, which raise concerns about the environmental impact caused by the integration of large scale photovoltaic facilities. Even though power from PV has a low global warming potential (GWP) according to several life cycle assessments (LCA) summarized in [63], the integration of these systems can require a complex set of environmental trade-offs. To understand the real environmental impact of the integration of these large photovoltaic facilities, the whole life cycle of the plant needs to be considered, from the extraction of the raw materials to the decommissioning and disposal of the PV system.

PV power plants have negative repercussions in the ecosystem, particularly in wildlife and habitat, land use, soils and water resources. The principal influence on biodiversity is due to the land occupation by the PVPPs and LS-PVPPs. Therefore, it is crucial to investigate and select the most appropriate location for these systems to avoid these problems [64].

Additionally, the use of hazardous materials in the manufacturing of the PV panels or inverters, among others, have to be taken into account together with the operation processes.

Finally, concerning the decommissioning stage, proper waste management (PV panels and other equipment) must be ensured to cause the minimum adverse environmental impact.

# Chapter 7

# Budget

The project budget is presented. The project has lasted from the 15th of February to the 22nd of June, 5 months length.

Table 7.2 shows the costs and hours associated with each phase of the project.

Table 7.1: Budget associated to human resources

| Concept | Price per hour | Hours | Total |
|---|---|---|---|
| Research | 40 € / h | 250 | 10000 |
| Development | 40 € / h | 200 | 8000 |
| Simulations | 40 € / h | 200 | 8000 |
| Writing | 40 € / h | 150 | 6000 |
| Total | | | 32000 € |

Table 7.2 shows the costs associated with hardware and software resources.

Table 7.2: Budget associated to hardware and software resources

| Concept | Price per unit | Units | Total |
|---|---|---|---|
| Computer | 600 € | 1 | 600 |
| OpenModelica | Free | 1 | Free |
| Total | | | 600 |

Therefore, the total cost of the project is of 32600 €.

# References

[1] Jäger-Waldau, A., PV Status Report 2018, EUR 29463 EN, Publications Office of the European Union, Luxembourg, 2018, ISBN 978-92-79-97465-6, doi:10.2760/826496, JRC113626

[2] "Solar power - Energy European Commission", *Energy - European Commission*, 2020. [Online]. Available: https://ec.europa.eu/energy/topics/renewable-energy/solar-power_en

[3] "EU solar boom: over 100% solar market increase in 2019", *Solarpowereurope.org*, 2020. [Online]. Available: https://www.solarpowereurope.org/eu-solar-boom-over-100-solar-market-increase-in-2019/

[4] C. Nayar, S. Islam, H. Dehbonei, K. Tan and H. Sharma, "Power Electronics for Renewable Energy Sources", *Alternative Energy in Power Electronics*, pp. 1-79, 2011. Available: 10.1016/b978-0-12-416714-8.00001-9

[5] V. Yaramasu, M. Rivera, A. Dekka and J. Rodriguez, "Predictive Control of Four-Leg Converters for Photovoltaic Energy Systems", *Power Systems*, pp. 45-69, 2019. Available: 10.1007/978-981-13-6151-7_3

[6] C. Verdugo, J. Candela, A. Luna and P. Rodriguez, "Power station for large scale photovoltaic power plants", *2017 IEEE 6th International Conference on Renewable Energy Research and Applications (ICRERA)*, 2017. Available: 10.1109/icrera.2017.8191163

[7] S. Kouro, J. I. Leon, D. Vinnikov and L. G. Franquelo "Grid-Connected Photovoltaic Systems: An Overview of Recent Research and Emerging PV Converter Technology," in IEEE Industrial Electronics Magazine, vol. 9, no. 1, pp. 47-61, March 2015.

[8] T. Ackermann, N. Martensen, T. Brown, P. Schierhorn (Energynautics GmbH), F. Boshell, F. Gafaro and M. Ayuso (IRENA). "Scaling up variable renewable power: the role of grid codes" International Renewable Energy Agency (IRENA), 2016. [Online] Available: www.irena.org/Publications

[9] A. Cabrera-Tobar, E. Bullich-Massagué, M. Aragüés-Peñalba and O. Gomis-Bellmunt, "Review of advanced grid requirements for the integration of large scale photovoltaic power plants in the transmission system", *Renewable and Sustainable Energy Reviews*, vol. 62, pp. 971-987, 2016. Available: 10.1016/j.rser.2016.05.044

[10] M. Obi and R. Bass, "Trends and challenges of grid-connected photovoltaic systems A review," Renew. Sustain. Energy Rev., vol. 58, pp. 1082–1094, may 2016.

[11] A. Cabrera-Tobar, E. Bullich-Massagué, M. Aragüés-Peñalba and O. Gomis-Bellmunt, "Active and Reactive Power Control of a PV Generator for Grid Code Compliance", *Energies*, vol. 12, no. 20, p. 3872, 2019. Available: 10.3390/en12203872

[12] E. Rakhshani, K. Rouzbehi, A. J. Sánchez, A. Tobar and E. Pouresmaeil, "Integration of Large Scale PV-Based Generation into Power Systems: A Survey", *Energies*, vol. 12, no. 8, p. 1425, 2019. Available: 10.3390/en12081425

[13] L. Hassaine, E. OLias, J. Quintero and V. Salas, "Overview of power inverter topologies and control structures for grid connected photovoltaic systems", *Renewable and Sustainable Energy Reviews*, vol. 30, pp. 796-807, 2014. Available: 10.1016/j.rser.2013.11.005

[14] A. Cabrera-Tobar, E. Bullich-Massagué, M. Aragüés-Peñalba, O. Gomis-Bellmunt, "Topologies for large scale photovoltaic power plants", Renewable and Sustainable Energy Reviews., 59 (2016),pp. 309-309

[15] J. Rodriguez, L. Franquelo, S. Kouro, J. Leon, R. Portillo, M. Prats, and M. Perez, "Multilevel Converters: An Enabling Technology for High-Power Applications," Proc. IEEE, vol. 97, no. 11, pp. 1786–1817, Nov. 2009

[16] A. Cabrera-Tobar, "Large scale photovoltaic power plants: configuration, integration and control". Tesi doctoral, UPC, Departament d'Enginyeria Elèctrica, 2018. [Online] Available: http://hdl.handle.net/2117/120996

[17] S. AG, "PV Inverters - Basic Facts for Planning PV Systems", *Sma.de*, 2020. [Online]. Available: https://www.sma.de/en/partners/knowledgebase/pv-inverters-basic-facts-for-planning-pv-systems.html

[18] S. Testa, A. De Caro and T. Scimone, "Sizing of step-up transformers for PV plants through a Probabilistic Approach." [Online]. Available: http://www.wseas.org

[19] "Requirements for Medium-Voltage Transformers and Transformers for Internal Power Supply for SUNNY CENTRAL." [Online]. Available: http://files.sma.de

[20] D. A. Trevas, A. Peterson, K. J. Rapp, and J. Luksich, "Optimal sizing of solar energy transformers using natural ester fluid," in 2012 11th Int. Conf. Environ. Electr. Eng. IEEE, May 2012, pp. 1006–1010.

[21] Openmodelica.org. 2020. *Welcome To Openmodelica - Openmodelica*. [Online] Available at: https://openmodelica.org/

[22] "Modelica Language — Modelica Association", *Modelica.org*, 2020. [Online]. Available: https://www.modelica.org/modelicalanguage

[23] P. Fritzson, *Principles of Object-Oriented Modeling and Simulation with Modelica 3.3: A Cyber-Physical Approach*. Institute of Electrical and Electronics Engineers, Inc., 2015.

[24] D. Winkler, "Electrical Power System Modelling in Modelica - Comparing Open-source Library Options", *Proceedings of the 58th Conference on Simulation and Modelling (SIMS 58) Reykjavik, Iceland, September 25th – 27th, 2017*, 2017. Available: 10.3384/ecp17138263

[25] F. Casella, "Simulation of Large-Scale Models in Modelica: State of the Art and Future Perspectives", *Proceedings of the 11th International Modelica Conference, Versailles, France, September 21-23, 2015*, 2015. Available: 10.3384/ecp15118459

[26] F. Casella, A. Bartolini, S. Pasquini and L. Bonuglia, "Object-oriented modelling and simulation of large-scale electrical power systems using Modelica: A first feasibility study," *IECON 2016 - 42nd Annual Conference of the IEEE Industrial Electronics Society*, Florence, 2016, pp. 6298-6304, doi: 10.1109/IECON.2016.7793558

[27] F. Jorissen, M. Wetter and L. Helsen, "Simulation Speed Analysis and Improvements of Modelica Models for Building Energy Simulation", *Proceedings of the 11th International Modelica Conference, Versailles, France, September 21-23, 2015*, 2015. Available: 10.3384/ecp1511859

[28] W. Braun, F. Casella and B. Bachmann, "Solving large-scale Modelica models: new approaches and experimental results using OpenModelica", *Proceedings of the 12th International Modelica Conference, Prague, Czech Republic, May 15-17, 2017*, 2017. Available: 10.3384/ecp17132557

[29] "Solving Modelica Models — OpenModelica User's Guide v1.16.0-dev-455-gb5354d94d9 documentation", *Openmodelica.org*, 2020. [Online]. Available: https://openmodelica.org

[30] E. Henningsson, H. Olsson and L. Vanfretti, "DAE Solvers for Large-Scale Hybrid Models", *Proceedings of the 13th International Modelica Conference, Regensburg, Germany, March 4–6, 2019*, 2019. Available: 10.3384/ecp19157491

[31] A. Pop, B.Thiele “Develop efficient multicore simulation” Open Cyber-Physical System Model-Driven Certified Development. ITEA3 Project no. 14018. , 2017. [Online] Available: http://itea3.org

[32] K. Abdelhak, B. Bachmann, F. Rosière, A.Guironnet “Experience on the use of the DAE mode in industrial power system simulations” [Online] Available: https://openmodelica.org

[33] G. Agosta, E. Baldino, F. Casella, S. Cherubin, A. Leva and F. Terraneo, "Towards a High-Performance Modelica Compiler", *Proceedings of the 13th International Modelica Conference, Regensburg, Germany, March 4–6, 2019*, 2019. Available: 10.3384/ecp19157313

[34] M. Sjölund, R. Braun, P. Fritzson, P. Krus. “Towards Efficient Distributed Simulation in Modelica using Transmission Line Modeling”. In: Proceedings of the 3rd International Workshop on Equation-Based Object-Oriented Modeling Languages and Tools. Ed. by P.Fritzson, E. Lee, F. Cellier, D. Broman. Oslo, Norway: Linköping University Electronic Press, Oct. 2010, pp. 71–80. url: http://www.ep.liu.se/ecp/047/

[35] B. Eriksson, P. Nordin, P. Krus "Hopsan, A C++ Implementation Utilising TLM Simulation Technique". In: Proceedings of the 51st Conference on Simulation and Modelling (SIMS). Oulu, Finland, Oct. 2010.

[36] L. Ochel et al., "OMSimulator - Integrated FMI and TLM-based Co-simulation with Composite Model Editing and SSP", *Proceedings of the 13th International Modelica Conference, Regensburg, Germany, March 4–6, 2019*, 2019. Available: 10.3384/ecp1915769

[37] "FMI and TLM-Based Simulation and Co-simulation of External Models — OpenModelica User's Guide v1.16.0-dev-477-g4023d498ac documentation", *Openmodelica.org*, 2020. [Online]. Available: https://www.openmodelica.org/doc/OpenModelicaUsersGuide/latest/fmitlm.html

[38] P. Aronsson. "Automatic Parallelization of Equation-Based Simulation Programs". PhD thesis, Linköping University, Department of Computer and Information Science, 2006.

[39] F. Casella "A Strategy for Parallel Simulation of Declarative Object-Oriented Models of Generalized Physical Networks." *EOOLT*, 2013.

[40] M. Walther, V. Waurich, C. Schubert and I. Gubsch, "Equation based parallelization of Modelica models", *Proceedings of the 10th International Modelica Conference, March 10-12, 2014, Lund, Sweden*, 2014. Available: 10.3384/ecp140961213

[41] M. Mothes, "hpcom_home: Home", *Hpc-om.de*, 2020. [Online]. Available: https://hpc-om.de/index.php?id=6

[42] "Task-Graph-Based Parallelization of Modelica-Simulations" [Online] Available: https://hpc-om.de/fileadmin/user_upload/HPCOM-Tutorial.pdf

[43] H. Elmqvist, S. Mattsson and H. Olsson, "Parallel Model Execution on Many Cores", *Proceedings of the 10th International Modelica Conference, March 10-12, 2014, Lund, Sweden*, 2014. Available: 10.3384/ecp14096363

[44] M. Gebremedhin, 'Automatic and Explicit Parallelization Approaches for Equation Based Mathematical Modeling and Simulation', PhD dissertation, Linköping University Electronic Press, Linköping, 2018.

[45] A. Egea-Alvarez, A. Junyent-Ferré, and O. Gomis-Bellmunt, Modeling and Control of Sustainable Power Systems (editor Wang L.), ch. "Active and Reactive Power Control of Grid Connected Distributed Generation Systems", pp. 47–81. Green Energy and Technology, Springer, Berlin, Heidelberg, 2012.

[46] R. Teodorescu, M. Liserre and P. Rodriguez, *Grid converters for photovoltaic and wind power systems*. Chichester, U.K.: Wiley, 2011.

[47] L. Harnefors and H. -. Nee, "Model-based current control of AC machines using the internal model control method," in *IEEE Transactions on Industry Applications*, vol. 34, no. 1, pp. 133-141, Jan.-Feb. 1998, doi: 10.1109/28.658735

[48] F. Blaabjerg, R. Teodorescu, M. Liserre and A. V. Timbus, "Overview of Control and Grid Synchronization for Distributed Power Generation Systems," in IEEE Transactions on Industrial Electronics, vol. 53, no. 5, pp. 1398-1409, Oct. 2006, doi: 10.1109/TIE.2006.881997

[49] S. K. Chung "A phase tracking system for three phase utility interface inverters", *IEEE Transactions on Power Electronics*, vol. 15, no. 3, pp. 431-438, 2000. Available: 10.1109/63.844502

[50] M. Ito, Kato, Komoto, Kichimi, and Kurokawa, "A Sensitivity Analysis of Very Large-Scale Photovoltaic Power Generation (VLS-PV) Systems in Deserts," in *2006 IEEE 4th World Conference on Photovoltaic Energy Conference*, 2006, vol. 2, pp. 2387–2390, doi: 10.1109/WCPEC.2006.279672

[51] D. Leanardič. "Large-Scale Photovoltaic Power Plants, Annual and Cumulative Installed Power Output Capacity" [Online] Available: https://www.pvresources.com

[52] "Solarfeld beseitigt Altlasten", *MOZ.de*, 2020. [Online]. Available: https://www.moz.de/artikel-ansicht/dg/0/1/1037444/

[53] S. AG, "Templin, Germany", *Sma.de*, 2020. [Online]. Available: https://www.sma.de/en/products/references/templin-germany.html

[54] E. Bullich-Massagué, O. Gomis-Bellmunt, L. Serrano-Salamanca, R. Ferrer-San-José, C. Pacheco-Navas and M. Aragüés-Peñalba, "Power plant control in large-scale photovoltaic plants: design, implementation and validation in a 9.4 MW photovoltaic plant", *IET Renewable Power Generation*, vol. 10, no. 1, pp. 50-62, 2016. Available: 10.1049/iet-rpg.2015.0113

[55] "SUNNY CENTRAL 800CP XT / 850CP XT / 900CP XT" [Online]. Available: http://files.sma.de

[56] "Short Circuit Fault Calculations." [Online]. Available: fs.fed.us/database/acad/elec/greenbook/10_shortcalc.pdf

[57] IEC 60076-5:2000(E) Power transformers – Part 5: Ability to withstand short circuit. [Online] Available: https://www.iec.ch

[58] "6-36kV Medium Voltage Underground Power Cables" [Online] Available at: www.powercables.com

[59] R. Villà Millaruelo, *Dinàmica de sistemes*. Barcelona: ETSEIB. CPDA, 2000.

[60] "#5960 (Large scale electrical models) – OpenModelica", *Trac.openmodelica.org*, 2020. [Online]. Available: https://trac.openmodelica.org/OpenModelica/ticket/5960#comment:6. [Accessed: 14- Jun- 2020].

[61] "#5452 (Numerical issues due to missing index reduction) – OpenModelica", *Trac.openmodelica.org*, 2020. [Online]. Available: https://trac.openmodelica.org/OpenModelica/ticket/5452. [Accessed: 14- Jun- 2020].

[62] "OpenModelica Compiler Flags — OpenModelica User's Guide v1.16.0-dev-455-gb5354d94d9 documentation", *Openmodelica.org*, 2020. [Online]. Available: https://www.openmodelica.org

[63] L. Stamford and A. Azapagic, "Environmental Impacts of Photovoltaics: The Effects of Technological Improvements and Transfer of Manufacturing from Europe to China", *Energy Technology*, vol. 6, no. 6, pp. 1148-1160, 2018. Available: 10.1002/ente.201800037

[64] B. Saracoglu et al., "A framework for selecting the location of very large photovoltaic solar power plants on a global/supergrid", *Energy Reports*, vol. 4, pp. 586-602, 2018. Available: 10.1016/j.egyr.2018.09.002

[65] J. G. Bergas "Control del motor d'inducció considerant els límits del convertidor i del motor". Tesi doctoral, UPC, Departament d'Enginyeria Elèctrica, 2000. Available: http://hdl.handle.net/2117/93605

# Appendix A

# Park and Clarke transformations

## A.1 Park transformation

The Park transformation converts the time-domain components in the *abc* reference of a three-phase system to time-invariant direct-quadrature synchronous frame [31]. It is given by

$$[x_{qd0}] = [T_{qd0}][x_{abc}] \tag{A.1}$$

$$[x_{abc}] = [T_{qd0}]^{-1}[x_{qd0}] \tag{A.2}$$

The transformation matrix can be written as

$$T_{qd0}(\theta) = \frac{2}{3}\begin{bmatrix} cos(\theta) & cos\left(\theta - \frac{2\pi}{3}\right) & cos\left(\theta + \frac{2\pi}{3}\right) \\ sin(\theta) & sin\left(\theta - \frac{2\pi}{3}\right) & sin\left(\theta + \frac{2\pi}{3}\right) \\ \frac{1}{2} & \frac{1}{2} & \frac{1}{2} \end{bmatrix} \tag{A.3}$$

and its inverse,

$$T_{qd0}^{-1}(\theta) = \begin{bmatrix} cos(\theta) & sin(\theta) & 1 \\ cos\left(\theta - \frac{2\pi}{3}\right) & sin\left(\theta - \frac{2\pi}{3}\right) & 1 \\ cos\left(\theta + \frac{2\pi}{3}\right) & sin\left(\theta + \frac{2\pi}{3}\right) & 1 \end{bmatrix} \tag{A.4}$$

## A.2 Clarke transformation

The Clarke transformation permits to transform sinusoidal three-phase to an orthogonal $\alpha\beta 0$ reference frame. Therefore, the Clarke transformation is defined as

$$[x_{\alpha\beta 0}] = [T_{\alpha\beta 0}][x_{abc}] \tag{A.5}$$

$$[x_{abc}] = [T_{\alpha\beta 0}]^{-1}[x_{\alpha\beta 0}] \tag{A.6}$$

Where $x_{abc}$ is the three-phase quantities vector in the $abc$ frame and $x_{\alpha\beta 0}$ is a vector with the transformed quantities in the $\alpha\beta 0$ frame. The transformation matrix can be written as

$$T_{\alpha\beta 0} = \frac{2}{3}\begin{bmatrix} 1 & -\frac{1}{2} & -\frac{1}{2} \\ 0 & -\frac{\sqrt{3}}{2} & \frac{\sqrt{3}}{2} \\ \frac{1}{2} & \frac{1}{2} & \frac{1}{2} \end{bmatrix} \tag{A.7}$$

and its inverse,

$$T_{\alpha\beta 0}^{-1} = \frac{2}{3}\begin{bmatrix} 1 & 0 & 1 \\ -\frac{1}{2} & -\frac{\sqrt{3}}{2} & 1 \\ -\frac{1}{2} & \frac{\sqrt{3}}{2} & 1 \end{bmatrix} \tag{A.8}$$

# Appendix B

# Space Vector Pulse Width Modulation

The Space Vector Pulse Width Modulation (SVPWM) technique is one of the most popular modulation approaches for two-level converters due to a high DC bus voltage use and it is well suited for digital implementation [45]. The concept of the SVPWM relies on the representation of the converter output AC voltages as space vectors [65]. Considering a two-level three-phase converter, $2^3 = 8$ switching states are obtained. The distribution of the voltage vectors for the eight switching states in the $\alpha\beta$ reference can be represented as

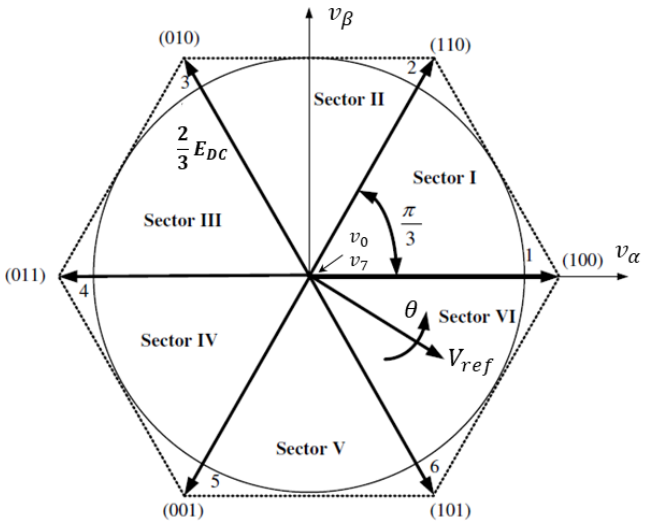


Figure B.1: Space Vector hexagon representation

Where $v_0$ and $v_7$ are denominated as zero vectors and $v_1$ to $v_6$ are denominated as active vectors. SVPWM is based on the application of these vectors during each switching period of duration $T_s = 1/f_{sw}$.

To calculate the connection time for each vector the reference voltage module and angle are computed as

$$V_{ref} = \sqrt{v_\alpha^2 + v_\beta^2} \tag{B.1}$$

$$\theta_{ref} = \arctan\frac{v_\alpha}{v_\beta} \tag{B.2}$$

If the angle is not located in the first sector, it can be reduced to it by

$$\theta_{sec1} = \theta_{ref} - \frac{\pi}{3}(n-1) \tag{B.3}$$

where $n$ is the sector where the desired voltage is.

The modulation times *t1* and *t2* for the vectors 1 and 2 can be calculated as [28]

$$t_1 = \frac{\sqrt{3}V_{ref}}{2E_{DC}} T_s \sin\left(\frac{\pi}{3} - \theta_{sec1}\right) \tag{B.4}$$

$$t_2 = \frac{\sqrt{3}V_{ref}}{2E_{DC}} T_s \sin(\theta_{sec1}) \tag{B.5}$$

The rest of the period is distributed as

$$t_{v0} = t_{v7} = T - t_1 - t_2 \tag{B.6}$$

A continuous SVPWM Modelica code to generate the inverter switching pattern has been developed in Modelica language. The code has been first developed and tested in Python and afterwards translated to Modelica. The height and width of the saw tooth signal used to compare the corresponding commutation with the time are equal to $T_s$. Regarding the converter branches (Fig. 2.1), *sa* represents the first (gates s1 and s2); *sb* represents the second (gates s3 and s4); and *sc* represents the third (gates s5 and s6). Then, the Modelica classes to generate the switching pattern for the converter are presented:

```
class ab_reference
  Modelica.Blocks.Interfaces.RealInput Valfa annotation( ...);
  Modelica.Blocks.Interfaces.RealInput Vbeta annotation( ...);
  Modelica.Blocks.Interfaces.RealOutput Vref annotation( ...);
  Modelica.Blocks.Interfaces.RealOutput thetaref annotation( ...);

  Real u;
  constant Real pi = Modelica.Constants.pi;
algorithm
  if Valfa == 0.0 then
    thetaref := 0.5 * pi;
    Vref := Vbeta;
  else
    u := Vbeta / Valfa;
    thetaref := atan(u);
    Vref := sqrt(Valfa ^ 2 + Vbeta ^ 2);
  end if;
  annotation( ...);
end ab_reference;
```

```
class svpwm
  Modelica.Blocks.Interfaces.RealInput signal annotation( ...);
  Modelica.Blocks.Interfaces.RealInput Vref annotation( ...);
  Modelica.Blocks.Interfaces.RealInput Thetaref annotation( ...);
  Modelica.Blocks.Interfaces.RealOutput sa annotation( ...);
  Modelica.Blocks.Interfaces.RealOutput sb annotation( ...);
  Modelica.Blocks.Interfaces.RealOutput sc annotation( ...);

  parameter Real Ts;
  parameter Real Edc;


  constant Real pi = Modelica.Constants.pi;
  Real t0;
  Real t1;
  Real t2;
  Real vectort[7];
  Real v1[7];
  Real v2[7];
  Real v3[7];
  Integer n;
  Real vcumsum[7];
  Real thetaref1;
algorithm
//sector I
  if 0 <= Thetaref and Thetaref < pi / 3 then
    thetaref1 := Thetaref;
    n := 1;
    t1 := sqrt(3) * Vref / (2 * Edc) * Ts * sin(pi / 3 - Thetaref);
    t2 := sqrt(3) * Vref / (2 * Edc) * Ts * sin(Thetaref);
    t0 := Ts - t1 - t2;
    vectort := {t0 / 4, t1 / 2, t2 / 2, t0 / 2, t2 / 2, t1 / 2, t0 / 4};
    vcumsum := {vectort[1], vectort[1] + vectort[2], vectort[1] + vectort[2] + vectort[3], vectort[1] +
vectort[2] + vectort[3] + vectort[4], vectort[1] + vectort[2] + vectort[3] + vectort[4] + vectort[5], vectort[1]
+ vectort[2] + vectort[3] + vectort[4] + vectort[5] + vectort[6], vectort[1] + vectort[2] + vectort[3] +
vectort[4] + vectort[5] + vectort[6] + vectort[7]};
    v1 := {0, 1, 1, 1, 1, 1, 0};
    v2 := {0, 0, 1, 1, 1, 0, 0};
    v3 := {0, 0, 0, 1, 0, 0, 0};
    for i in 1:7 loop
      if signal < vcumsum[i] then
        sa := v1[i];
        sb := v2[i];
        sc := v3[i];
        break;
      end if;
    end for;
  end if;
//sector II
  if pi / 3 <= Thetaref and Thetaref < 2 * pi / 3 then
    n := 2;
    thetaref1 := Thetaref - pi / 3 * (n - 1);
    t1 := sqrt(3) * Vref / (2 * Edc) * Ts * sin(pi / 3 - thetaref1);
    t2 := sqrt(3) * Vref / (2 * Edc) * Ts * sin(thetaref1);
    t0 := Ts - t1 - t2;
    vectort := {t0 / 4, t1 / 2, t2 / 2, t0 / 2, t2 / 2, t1 / 2, t0 / 4};
    vcumsum := {vectort[1], vectort[1] + vectort[2], vectort[1] + vectort[2] + vectort[3], vectort[1] +
vectort[2] + vectort[3] + vectort[4], vectort[1] + vectort[2] + vectort[3] + vectort[4] + vectort[5], vectort[1]
+ vectort[2] + vectort[3] + vectort[4] + vectort[5] + vectort[6], vectort[1] + vectort[2] + vectort[3] +
vectort[4] + vectort[5] + vectort[6] + vectort[7]};
    v1 := {0, 0, 1, 1, 1, 0, 0};
    v2 := {0, 1, 1, 1, 1, 1, 0};
    v3 := {0, 0, 0, 1, 0, 0, 0};
    for i in 1:7 loop
      if signal < vcumsum[i] then
        sa := v1[i];
        sb := v2[i];
        sc := v3[i];
        break;
      end if;
    end for;
  end if;
```

Listing - Continued

```
//sector III
  if 2 * pi / 3 <= Thetaref and Thetaref < pi then
    n := 3;
    thetaref1 := Thetaref - pi / 3 * (n - 1);
    t1 := sqrt(3) * Vref / (2 * Edc) * Ts * sin(pi / 3 - thetaref1);
    t2 := sqrt(3) * Vref / (2 * Edc) * Ts * sin(thetaref1);
    t0 := Ts - t1 - t2;
    vectort := {t0 / 4, t1 / 2, t2 / 2, t0 / 2, t2 / 2, t1 / 2, t0 / 4};
    vcumsum := {vectort[1], vectort[1] + vectort[2], vectort[1] + vectort[2] + vectort[3], vectort[1] +
vectort[2] + vectort[3] + vectort[4], vectort[1] + vectort[2] + vectort[3] + vectort[4] + vectort[5], vectort[1]
+ vectort[2] + vectort[3] + vectort[4] + vectort[5] + vectort[6], vectort[1] + vectort[2] + vectort[3] +
vectort[4] + vectort[5] + vectort[6] + vectort[7]};
    v1 := {0, 0, 0, 1, 0, 0, 0};
    v2 := {0, 1, 1, 1, 1, 1, 0};
    v3 := {0, 0, 1, 1, 1, 0, 0};
    for i in 1:7 loop
      if signal < vcumsum[i] then
        sa := v1[i];
        sb := v2[i];
        sc := v3[i];
        break;
      end if;
    end for;
  end if;
//sector IV
  if (-pi) <= Thetaref and Thetaref < (-2 * pi / 3) then
    n := 4;
    thetaref1 := Thetaref - pi / 3 * (n - 1);
    t1 := sqrt(3) * Vref / (2 * Edc) * Ts * sin(pi / 3 - thetaref1);
    t2 := sqrt(3) * Vref / (2 * Edc) * Ts * sin(thetaref1);
    t0 := Ts - t1 - t2;
    vectort := {t0 / 4, t1 / 2, t2 / 2, t0 / 2, t2 / 2, t1 / 2, t0 / 4};
    vcumsum := {vectort[1], vectort[1] + vectort[2], vectort[1] + vectort[2] + vectort[3], vectort[1] +
vectort[2] + vectort[3] + vectort[4], vectort[1] + vectort[2] + vectort[3] + vectort[4] + vectort[5], vectort[1]
+ vectort[2] + vectort[3] + vectort[4] + vectort[5] + vectort[6], vectort[1] + vectort[2] + vectort[3] +
vectort[4] + vectort[5] + vectort[6] + vectort[7]};
    v1 := {0, 0, 0, 1, 0, 0, 0};
    v2 := {0, 0, 1, 1, 1, 0, 0};
    v3 := {0, 1, 1, 1, 1, 1, 0};
    for i in 1:7 loop
      if signal < vcumsum[i] then
        sa := v1[i];
        sb := v2[i];
        sc := v3[i];
        break;
      end if;
    end for;
  end if;
//sector V
  if (-2 * pi / 3) <= Thetaref and Thetaref < (-pi / 3) then
    n := 5;
    thetaref1 := Thetaref - pi / 3 * (n - 1);
    t1 := sqrt(3) * Vref / (2 * Edc) * Ts * sin(pi / 3 - thetaref1);
    t2 := sqrt(3) * Vref / (2 * Edc) * Ts * sin(thetaref1);
    t0 := Ts - t1 - t2;
    vectort := {t0 / 4, t1 / 2, t2 / 2, t0 / 2, t2 / 2, t1 / 2, t0 / 4};
    vcumsum := {vectort[1], vectort[1] + vectort[2], vectort[1] + vectort[2] + vectort[3], vectort[1] +
vectort[2] + vectort[3] + vectort[4], vectort[1] + vectort[2] + vectort[3] + vectort[4] + vectort[5], vectort[1]
+ vectort[2] + vectort[3] + vectort[4] + vectort[5] + vectort[6], vectort[1] + vectort[2] + vectort[3] +
vectort[4] + vectort[5] + vectort[6] + vectort[7]};
    v1 := {0, 0, 1, 1, 1, 0, 0};
    v2 := {0, 0, 0, 1, 0, 0, 0};
    v3 := {0, 1, 1, 1, 1, 1, 0};
    for i in 1:7 loop
      if signal < vcumsum[i] then
        sa := v1[i];
        sb := v2[i];
        sc := v3[i];
        break;
      end if;
    end for;
  end if;
```

Listing - Continued

```
//sector VI
  if (-pi / 3) <= Thetaref and Thetaref < 0 then
    n := 6;
    thetaref1 := Thetaref - pi / 3 * (n - 1);
    t1 := sqrt(3) * Vref / (2 * Edc) * Ts * sin(pi / 3 - thetaref1);
    t2 := sqrt(3) * Vref / (2 * Edc) * Ts * sin(thetaref1);
    t0 := Ts - t1 - t2;
    vectort := {t0 / 4, t1 / 2, t2 / 2, t0 / 2, t2 / 2, t1 / 2, t0 / 4};
    vcumsum := {vectort[1], vectort[1] + vectort[2], vectort[1] + vectort[2] + vectort[3], vectort[1] +
vectort[2] + vectort[3] + vectort[4], vectort[1] + vectort[2] + vectort[3] + vectort[4] + vectort[5], vectort[1]
+ vectort[2] + vectort[3] + vectort[4] + vectort[5] + vectort[6], vectort[1] + vectort[2] + vectort[3] +
vectort[4] + vectort[5] + vectort[6] + vectort[7]};
    v1 := {0, 1, 1, 1, 1, 1, 0};
    v2 := {0, 0, 0, 1, 0, 0, 0};
    v3 := {0, 0, 1, 1, 1, 0, 0};
    for i in 1:7 loop
      if signal < vcumsum[i] then
        sa := v1[i];
        sb := v2[i];
        sc := v3[i];
        break;
      end if;
    end for;
  end if;
equation

  annotation( ...);
end svpwm;
```

```
class switching_pattern
  Modelica.Blocks.Interfaces.RealInput sa annotation( ...);
  Modelica.Blocks.Interfaces.RealInput sb annotation( ...);
  Modelica.Blocks.Interfaces.RealInput sc annotation( ...);
  Modelica.Blocks.Interfaces.BooleanOutput s1 annotation( ...);
  Modelica.Blocks.Interfaces.BooleanOutput s2 annotation( ...);
  Modelica.Blocks.Interfaces.BooleanOutput s3 annotation( ...);
  Modelica.Blocks.Interfaces.BooleanOutput s4 annotation( ...);
  Modelica.Blocks.Interfaces.BooleanOutput s5 annotation( ...);
  Modelica.Blocks.Interfaces.BooleanOutput s6 annotation( ...);
algorithm
  if sa == 1 then
    s1 := true;
    s2 := false;
  else
    s1 := false;
    s2 := true;
  end if;
  if sb == 1 then
    s3 := true;
    s4 := false;
  else
    s3 := false;
    s4 := true;
  end if;
  if sc == 1 then
    s5 := true;
    s6 := false;
  else
    s5 := false;
    s6 := true;
  end if;
  annotation( ...);
end switching_pattern;
```